Volume: 23/ 1&2

MARCH 2011

ISRAPS Bulletin

NSRP - 2011 SPECIAL ISSUE

STRUCTURE & DYNAMICS OF COMPLEX CHEMICAL SYSTEMS: AN INTERFACE BETWEEN THEORY & EXPERIMENT

ISRAPS

Guest Editor

Dr. Chandra N Patra

A Publication of

Indian Society For

Radiation & Photochemical Sciences

ISRAPS Bulletin

A Publication of
Indian Society for Radiation and Photochemical Sciences

Editorial

Dear Fellow Members,

'Chemistry: An Experimental Science' is a part of the 'Chemistry' syllabus in junior colleges all over India. That 'Chemistry' has developed from old days 'Alchemy' is known over the years. However, processes leading to 'Alchemy' or 'Chemistry' are thought experiments, better known as 'Simulations' in the present days. Such thought experiments carried out on the basis of trial and error or rather stochastic methods led to the developments of robust deterministic approaches in recent times. This is indeed thought provoking to discuss such an issue among the scientists of mutual interest in an intriguing manner.

The ISRAPS Discussion Meeting on "Structure & Dynamics of Complex Chemical Systems: An Interface between Theory & Experiment" aims at bringing experimental as well as theoretical chemists together for an intense discussion on various scientific issues of mutual interest to enhance our understanding of complex chemical systems and phenomena. As is well known, the primary goal of theoretical chemistry is to provide an understanding and rationalization of the observed chemical phenomena as well as to predict new phenomena by developing concepts or performing computations with the help of the available theoretical, modeling or simulation techniques. Formulation of new and more powerful theoretical tools, modeling strategies or simulation techniques thus forms an ongoing and integral part of research activities in theoretical chemistry. Proposing new experiments, guided by theoretical insight, also constitute a valuable component of research in theoretical chemistry.

With the availability of powerful computational resources, large scale computer simulation of the behaviour of complex systems has attracted more emphasis and the challenging task of computational design of new molecules and novel materials with tailor made properties has gained momentum.

The present meeting is expected to provide a stimulating environment and suitable platform for fruitful discussion and exchange of ideas leading to the emergence of new concepts. This is expected to open up new windows to bring in fresh flavour of collaborative and interdisciplinary character in the chemistry research activities involving a synergy between theory, modeling, simulation and experiments.

Chandra N. Patra *(Guest Editor)*
Theotical Chemistry Section
Bhabha Atomic Research Centre, Mumbai

Dr. Chandra N. Patra *is working as a senior scientist in the Theoretical Chemistry Section of Bhabha Atomic Research Centre. He graduated in Chemistry discipline from the 33rd batch of BARC Training School in 1989. Since then he is actively engaged in research and development work on the theoretical chemistry of soft condensed systems including designing of efficient methodologies and application to the areas of current interest. He obtained his Ph.D. in Chemistry from Bombay University in 1996 and has a large number of publications to his credit. He was a visiting professor at the Universidad de Guanajuato, Mexico in 2002 and an associate at the University of Utah, USA in 2005. He is a recipient of DAE Scientific & Technical Excellence Award.*

INDIAN SOCIETY FOR RADIATION AND PHOTOCHEMICAL SCIENCES
(Reg. No. 617/1985, GBBSD, Bombay; Trust No. F-10965) (Affiliated to IARR)
Radiation & Photochemistry Division
Bhabha Atomic Research Centre, Mumbai - 400 085

ISRAPS

Member Enrolment Form

1. Name in Block Letters:

2. Date of Birth:

3. Highest Academic Qualification:

4. Present Position:

5. Addresses:

Photograph

Office	Residence
Put your address here Telephone Fax E-mail	Put your address here Telephone Fax E-mail

6. Address for Correspondence: Office / Residence

7. Category of Membership Applied for: Annual / Life / corporate member

8. Remittance (DD only) payable to ISRAPS, Mumbai

Category	Fees	Admission fee	Total Amount
Annual	Rs 200/-	Rs 100/-	Rs 300/-
Life Member	Rs 1500/-	Rs 100/-	Rs 1600/-
Corporate Member	Rs 20000/-	Rs 1000/-	Rs 21000/-

9. Brief Resume of activities and research interests:

10. List of memberships of other professional bodies, if any:

11. List of prizes/awards/fellowships received, if any:

12. Number of Publications:

I agree to abide by the constitution and bye-laws, and rules and regulations of the SOCIETY.

Place: Signature

Date

Message from the President and Secretary

Dear Members of ISRAPS and Readers,

Greetings from the Executive Council of ISRAPS for a very happy and prosperous new year 2011! The year 2010 ended with holding the third Asia Pacific Symposium on Radiation Chemistry in conjunction with the tenth Trombay Symposium on Radiation & Photochemistry (TSRP-2010) at Lonavala, Maharashtra. It was a great success with 330 participants including about 80 overseas participants. In the year 2010 we had two ISRAPS Discussion Meetings on "Dye Sensitized Solar Cell" and "Supramolecular Chemistry" held in the month of January and April, respectively, in Mumbai. Leading experts in their respective areas delivered talks emphasizing current developments in both the field. More than 80 participants attended each of the meetings.

All our efforts in recent months have been focused on the preparation for organizing the National Symposium on Radiation & Photochemsitry to be held during March 10-12, 2011 at JNV University, Jodhpur. ISRAPS and the Department of Chemistry, JNV University, Jodhpur are jointly organizing this symposium. On behalf of ISRAPS and the symposium organizing committee, we welcome all the delegates to the symposium and wish them a very interactive and fruitful meeting. This is a special issue of ISRAPS Bulletin, which is being published on the eve of NSRP-2011. Finally, we would like to thank Dr. Chandra N Patra, the Guest Editor of this special issue, for his efforts in bringing out a scientifically rich issue of ISRAPS Bulletin containing six articles on the theme "Theory-Experiment Collaborative Research in Radiation & Photochemistry". Thanks are also due to all the authors for contributing articles.

We wish to express our gratitude to each and every member of ISRAPS for their continued support and cooperation in carrying out the activities of the society.

(Dr. Tulsi Mukherjee)
President

(Dr. Tapan K. Ghanty)
Secretary

Statistical Mechanical Description of Non-equilibrium Processes in Condensed Phase

Alok Samanta & Swapan Ghosh

Theoretical Chemistry Section, Bhabha Atomic Research Centre, Mumbai-400085, India

1. INTRODUCTION

Consider a many -particle system which at time zero is prepared in a non equilibrium state. If there is no constraint imposed on the system, at subsequent time the system would relax to the equilibrium state. To understand this relaxation process, let us assume that to every macroscopic observable $\alpha_j(t)$ (j=1,…..N) there corresponds a phase space function $A_j(G)$ such that

$$\alpha_j(t) = \int \rho(\Gamma, t)\, A_j \qquad (1)$$

where $\rho(\Gamma, t)$ is the probability density defined in Γ space, which represents the phase space co-ordinates of all the particles. If one knows what the time evolution equation for $\rho(\Gamma, t)$ is, one can in principle find the rate equations for the macroscopic variable $\alpha_j(t)$. Alternatively, one can evaluate α_j(t) as

$$\alpha_j(t) = \int \rho(\Gamma, 0)\, A_j \qquad (2)$$

where A_j(Γ,t) is given by

$$A_j(\Gamma,t)=\exp[-iLt]\, A_j \qquad (3)$$

with $\rho(\Gamma, 0)$ as the initially constrained probability distribution and L as the Liouville operator. In either scheme, it is important to have knowledge of the distribution function $\rho(\Gamma, 0)$ $\rho(\Gamma, 0)$. However, in many non-equilibrium situations, $\rho(\Gamma, 0)$ is unknown due to thermal fluctuations leading to new microscopic states for each repetition of the experiment with identical known initial macroscopic condition say $A(\Gamma_0) = \gamma_0$. If one starts with different initial phase space co-ordinate viz. $\Gamma_{01}, \Gamma_{02}, \ldots\ldots\ldots\ldots\Gamma_{0n}$ (all these different co-ordinates lie on the surface, defined by the equation $A(\Gamma_0) = \gamma_0$), corresponding to the same initial phase space functions viz. $A(\Gamma_{01}) = A(\Gamma_{02})\ldots\ldots\ldots\ldots\ldots A(\Gamma_{0n}) = \gamma_0$, one may encounter a different outcome of the system phase space points, viz. $\Gamma_1, \Gamma_2, \ldots\ldots\ldots\ldots\Gamma_n$, leading to the distinct phase space functions $A(\Gamma_1), A(\Gamma_2)\ldots\ldots\ldots\ldots\ldots A(\Gamma_n)$ for fixed observation time t as shown in figure 1.

The complete statistical description of the outcome of the repeated experiments is contained in the probability distribution $P(\gamma, t\,|\,\gamma_0, 0)$ of a microscopic phase space function A constrained to have a value γ at time t with its initial value γ_0 at $t = 0$. One can obtain the distribution $P(\gamma, t\,|\,\gamma_0, 0)$ from the knowledge of the phase space distribution function ρ(Γ, t) through the following transformation proposed by Zwanzig[1-4]

$$P(\gamma, t\,|\,\gamma_0, 0) = \int d\Gamma\, \delta(A(\Gamma) - \gamma)\, \rho(\Gamma, t) \quad . \qquad (4)$$

The kinetic equation for the probability distribution $P(\gamma, t\,|\,\gamma_0, 0)$, can be written as

$$\frac{\partial P(\gamma,t\,|\,\gamma_0,0)}{\partial t} = \frac{\partial}{\partial \gamma}\left[\int_0^t D(\gamma,\tau)\,d\tau\left[\frac{\partial P(\gamma,t-\tau\,|\,\gamma_0,0)}{\partial \gamma} + P(\gamma,t-\tau\,|\,\gamma_0,0)\frac{\partial}{\partial \gamma}\{\beta V^{eff}(\gamma)\}\right]\right] \qquad (5)$$

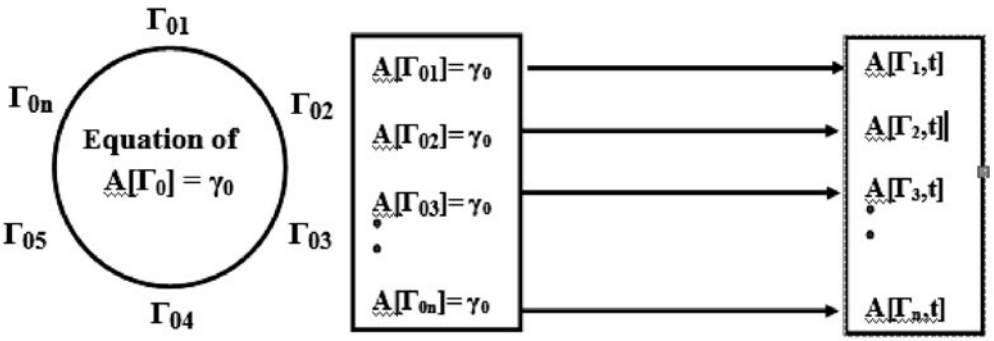

Figure 1 **:** *Outcome of different phase space functions* $A(\Gamma_1), A(\Gamma_2)\ldots\ldots\ldots\ldots A(\Gamma_n)$ *at time t for a given initial macroscopic condition say* $A(\Gamma_0) = \gamma_0$

Here, time- and γ-dependent diffusivity $D(\gamma,t)$ is defined as $D(\gamma,t)=\langle \dot{A}(t)\,\dot{A}(0)\,\delta(A(t)-\gamma)\rangle / \langle \delta(A(0)-\gamma)\rangle$, with the symbol $\langle --- \rangle$ denoting an equilibrium ensemble average and the dot corresponding to time derivative. The effective potential V^{eff}, a function of the γ coordinate, is defined as $\beta V^{eff}(\gamma) = -\ln C \langle \delta(A(0)-\gamma)\rangle$ where $\beta\,(=1/k_B T)$ denotes the inverse temperature and $C=\int_{-\infty}^{+\infty} d\gamma \exp\left[-\beta V^{eff}(\gamma)\right]$. Zwanzig's derivation of Eq. (5) assumes dA/dt to be small as has been discussed by him in details. If we want to calculate a particular property of $A(\Gamma)$, it is convenient to use the distribution function $P(\gamma,t\,|\,\gamma_0,0)$ corresponding to this quantity in contrast to the multi-dimensional phase space based approach discussed above. The generalized kinetic equation (Eq.5) provide a generalized approach for describing a wide class of dynamical phenomena viz. multi-dimensional electron transfer, non equilibrium solvation dynamics and escape of a particle from a potential well. Specifically, we consider here only two-dimensional electron transfer reactions.

Theory of Electron Transfer

In the general case, we may envisage the ET reaction as a multi-dimensional problem involving the reactant and the product surfaces. Here, the system is initially assumed to be in the reactant potential energy surface (PES) at time $t=0$. The ET reaction occurs when the population is transferred from the reactant PES to product PES and the intrinsic rate of transfer at the crossing region is given by k_0 corresponding to $\gamma=0$ i.e. when the reactant and product potential energies are equal. Hence the relevant microscopic phase-space function A for the ET reaction can be chosen to be the difference between the potential energy for the product (V^P) and that of the reactant (V^R), viz. $A=V^P-V^R$. Therefore, this has been employed in the kinetic equation for $P(\gamma,t\,|\,\gamma_0,0)$ given by Eq. (1) by modifying it for reversible ET reactions with introduction of a delta sink of strength k_0 to its right hand side for the forward as well as backward ET process. Thus, the kinetic equations that represent the situation are the following coupled equations of motion

$$\frac{\partial P(\gamma,t\,|\,\gamma_0,0)}{\partial t} = \frac{\partial}{\partial \gamma}\left\{\int_0^t D(\gamma,\tau)\,d\tau\left[\frac{\partial P(\gamma,t-\tau\,|\,\gamma_0,0)}{\partial \gamma} + P(\gamma,t-\tau\,|\,\gamma_0,0)\frac{\partial}{\partial \gamma}\{\beta V^{eff}(\gamma)\}\right]\right\} \quad (6)$$
$$-k_0\,\delta(\gamma)P(\gamma,k0\gamma_0\ \ )$$

where k_0 is the intrinsic rate and its expression can be written in terms of transfer integral J as $k_0=(4\pi^2/h)J^2$.

As an illustrative example, we now consider a typical ET reaction, where the system is assumed to be initially in the ground state and is brought to the non-equilibrium excited state by laser excitation. Subsequently, the system at the higher level of excitation relaxes downwards (towards the potential minimum of the excited-state surface) due to relaxation of the polar solvent till its energy coincides with that of the ground state where back electron transfer takes place. We consider here a simple theoretical model for the ET system of interest consisting of a two-dimensional space spanned by low frequency solvent polarization (X) and the vibrational coordinate (Q) or two low frequency solvent collective coordinates. Thus, we consider a standard low frequency harmonic oscillator model potential for the reactant and product systems defined respectively as

$$V^R(Q,X)=\frac{1}{2}Q^2+\frac{1}{2}X^2 \quad (7)$$

$$V^P(Q,X)=\frac{1}{2}(Q-Q_0)^2+\frac{1}{2}(X-X_0)^2+\Delta G \quad (8)$$

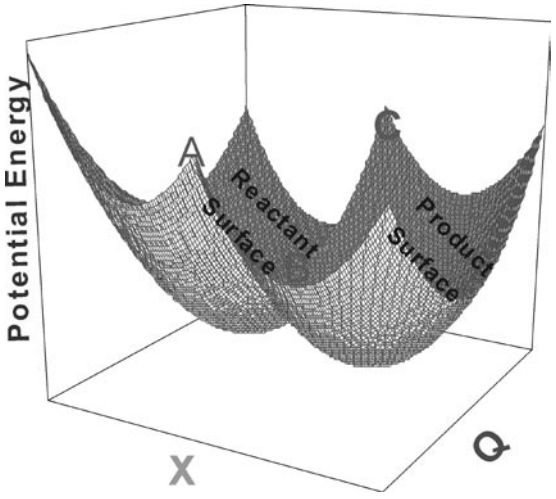

Figure 2 *: Potential energy surface of a two-dimensional electron transfer reaction. The two surfaces intersect on the curve ABC.*

and the phase space function A(t) for this potential is given by

$$A(t)=\lambda_T+\Delta G-(XX_0+QQ_0) \tag{9}$$

Here the total reorganization energy $\lambda_T(=\lambda_V+\lambda_S)$ is contributed by the low frequency vibrational and solvent reorganization energy $\lambda_V=(1/2)Q_0^2$ and $\lambda_S=(1/2)X_0^2$ respectively, while ΔG represents the free energy change of ET reaction. For this model, the effective potentials for the reactant and product can be respectively expressed as

$$\beta V_1^{eff}(\gamma)=\frac{\beta}{4\lambda_T}(\lambda_T+\Delta G-\gamma)^2 \tag{10}$$

$$\beta V_2^{eff}(\gamma)=\frac{\beta}{4\lambda_T}(-\lambda_T+\Delta G-\gamma)^2 \tag{11}$$

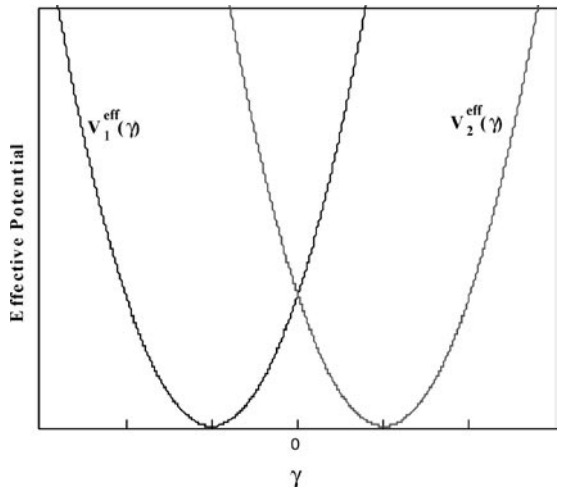

***Figure* 3 :** *Effective Potential Energy for the reactant and product. The abscissa stands for the one dimensional reaction coordinates* γ *. The ordinate stands for the effective potential. ET reaction takes place at the intersection point* $\gamma=0$.

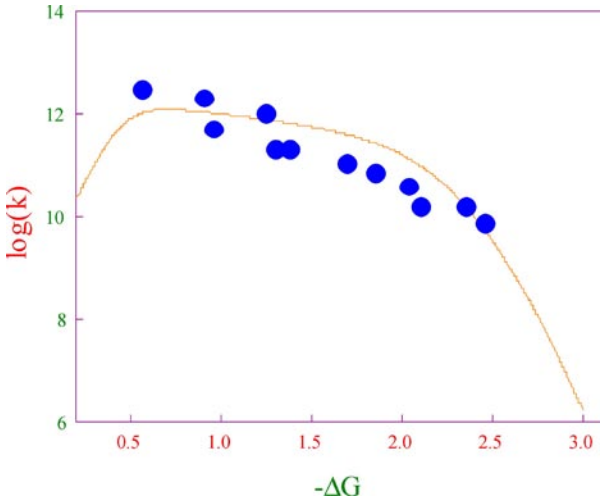

Figure 4: *Plot of the total rate constant k of back electron transfer for contact ion pairs (CIP) as a function of the free energy change (-ΔG). The parameters used are τ= 0.3 ps, J = 0.1 eV and T = 300 K. . The experimental data (•) correspond to the ET rate constant k and are taken from ref 5.*

In Figure 2, PES of the system is drawn in the two dimensional space spanned by the coordinates X and Q, with the curve ABC representing the intersection of the reactant and product PES, and ET takes place when the reactant reaches the intersection point. In Figure 3, we have plotted the potential energy of the reactant and product in one-dimensional γ-space. ET reaction takes place at the intersection point γ =0.

The analytical rate expression for the forward reaction k can be written as

$$k=\frac{k_{TST}}{\left[1+\frac{k_{TST}}{k_d}\right]} \tag{12}$$

and $k_i^d\left(=\tau_i^{-1}\right)$ corresponds to diffusion rate in i-th potential. k_{TST} and k_d represent respectively the rate of ET reaction calculated based on transition state theory and well dynamics, are defined as

$$k_{TST}=\frac{k_0}{(4\pi\lambda_T k_\beta T)^{1/2}}\exp\left[-\frac{\beta}{4\lambda_T}(\lambda_T+\Delta G)^2\right] \tag{13}$$

$$k_d^{-1}=(4\pi\lambda_T k_\beta T)^{1/2}\int_{z^*}^{z_0}dz\exp\left[z^2/4\lambda_T k_\beta T\right]\left(1-erf\left(z/(4\lambda_T k_\beta T)^{1/2}\right)\right)D(Z) \tag{14}$$

where k_0 is the intrinsic rate and its expression can be written in terms of transfer integral J as $k_0=(4\pi^2/h)J^2$, $z^*=(\lambda_T+\Delta G)$ and $z_0=2\lambda_T$. The position dependent diffusivity $D(z)=\int_0^\infty d\tau D(z,\tau)$ where $D(z,t)$ is defined as

$$D(Z,t)=\frac{2}{\beta}\left(\frac{\lambda_T}{B}\right)^{1/2}\frac{\exp\left[-\beta Z^2/4B\right]}{\exp\left[-\beta Z^2/4\lambda_T\right]}\times\left[\{\lambda_v f_1(t)(1/\tau_v)^2K_1\}+\{\lambda_v f_2(t)(1/\tau_s)^2K_2\}\right] \tag{15}$$

$$B=\lambda_v f_1^2(t)+\lambda_s f_2^2(t) \tag{16}$$

$$K_1=\left[1-\frac{\lambda_v f_1^2(t)}{B}\left(1-\frac{\beta Z^2}{2B}\right)\right] \tag{17}$$

$$K_2=\left[1-\frac{\lambda_s f_2^2(t)}{B}\left(1-\frac{\beta Z^2}{2B}\right)\right] \tag{18}$$

with $f_1(t) = \exp(-t/\tau_v)$ and $f_2(t) = \exp(-t/\tau_s)$. Here τ_v and τ_s are respectively represent the vibrational and polarization relaxation time. The rate expression derived here is quite general and involves the energy dependent diffusivity. We have calculated the rate constant k of back ET reactions using Eqs. (12)-(18) for contact ion pairs (CIP) in acetonitrile solvent as a function of the free energy change ΔG of the reaction. The solvent ralaxation time τ_v of acetonitrile is taken as 0.3 ps at temperature T = 300 K. For simplicity, we consider the relaxation time (τ_v) for the other mode to be same as τ_s. The one dimensional approach to multidimensional ET reactions developed here is applied to explain experimental results. The parameter used are: J= 0.3eV and λ_T =1.5 eV , $\tau_v = \tau_s = 0.3$ ps and temperature T = 300 k. The calculated results along experimental values are plotted in Fig.3

Concluding Remarks

The kinetic equation (Eq.5) provide a generalized approach for describing a wide class of dynamical phenomena. Specifically, we have considered here only two-dimensional electron transfer reactions in details. Calculated results for ET reactions is found to be very good in agreement with the available experimental results. Theory for non equilibrium solvation and escape of a particle from the potential well can easily be developed based on the generalized kinetic equation.

References

1. Zwanzig, R. *Phys. Re*V. **1961**, *124*, 983.
2. (a) Calef, D. F.; Wolynes, P. G. *J. Phys. Chem.* **1983**, *87*, 3387; (b) *J. Chem. Phys.* **1983**, *78*, 470.
3. Samanta, A.; Ghosh, S. K. *J. Phys. Chem. A* **2008**, *112*, 752.
4. Dhole, k.; Samanta, A.; Ghosh, S. K. *J. Phys. Chem. A* **2008**, *112*, 4879.
5. Asahi, T.; Mataga, N. *J. Phys. Chem.* **1991**, *95*, 1956.

Dr. Alok Kumar Samanta *joined B.A.R.C. in 1987 after graduating from the 30th course of BARC Training School in Chemistry discipline. He received his M.Sc. degree from I.I.T. Kharagpur and obtained Ph.D. degree from Bombay University in 2005. He is the recipient of DAE Scientific &Technical Excellence Award. His research interests include time-dependent density functional theory, mode- coupling theory, theory of electron transfer reactions, chemical dynamics and non equilibrium solvation in condensed phase. His recent work involves formulation of a unified one-dimensional approach to the multidimensional non equilibrium processes in condensed phase.*

Dr. Swapan K. Ghosh *received his Ph.D. in Chemistry from Indian Institute of Technology, Bombay in 1982. At present, he is Head of the Theoretical Chemistry Section, Bhabha Atomic Research Centre, Mumbai and is also Dean-Academic (BARC), Chemical Sciences, Homi Bhabha National Institute (Deemed University). His current research interests include density functional theory, multiscale materials modeling, computational materials science, dynamics in condensed phase and soft condensed matter physics. He is a Fellow of the Indian Academy of Sciences, Bangalore, Indian National Science Academy, New Delhi and National Academy of Sciences, India, Allahabad. He is the recipient of Third World Academy of Sciences (TWAS) prize in chemistry and also a fellow of TWAS.*

The Effect of Methyl Group Substitution on Hydrogen-Bonded Complexes of Phenylacetylene.

G. Naresh Patwari
Department of Chemistry, Indian Institute of Technology Bombay, Mumbai 400076
E-mail: naresh@chem.iitb.ac.in

Abstract

The infrared spectra in the acetylenic C–H stretching region for the complexes of phenylacetylene with water, methanol, and ammonia, methylamine are indicative of change in the intermolecular structure upon substitution with a methyl group. High-level ab-initio calculations at CCSD(T)/aug-cc-pVDZ level along with the SAPT calculations are used to rationalize the observed intermolecular structures. The changes in the intermolecular structure upon substitution with a methyl group can be attributed to the switching of the dominant interaction from electrostatic to dispersion.

Introduction

The vast majority of hydrogen bonding patterns observed in the crystal structures can be rationalized on the basis of Etter rules [1]. Similarly, based on rotationally resolved spectroscopy of several mixed dimers in the gas phase, Legon and Millen laid down rules for formation of X–H···B hydrogen bonding [2]. Both Etter and Legon-Millen rules suggest the hierarchy of hydrogen bond formation based on empirical observations and serve as guidelines to predict hydrogen bonding patterns [3]. However, in the case of multifunctional molecules, wherein multiple energetically closely spaced minima occur, the above rules perhaps cannot be used to predict the intermolecular structures. Phenylacetylene is perhaps the simplest multifunctional molecule to investigate competitive hydrogen bonding. It has three hydrogen bonding sites in the form of benzene ring and the acetylenic C≡C bond, which can act as π acceptors, and an activated acetylenic C–H group, which can act as a σ donor. Further, absence of any strongly acidic/basic functional groups renders the hierarchy of hydrogen bonding sites almost undeterminable. We have investigated several hydrogen bonded complexes of phenylacetylene with various solvent molecules such as water, methanol, ammonia, methylamine and other alcohols and amines [4-6]. These hydrogen-bonded complexes form a wide variety of intermolecular structures, which can be interpreted as subtle balance of intermolecular forces in various possible intermolecular structures. Most importantly, the intermolecular structures of the water and methanol complexes are different, similarly the structures of the ammonia and methylamine complexes are different. Such differences in the intermolecular structures of hydrogen-bonded complexes with water, methanol and ammonia, methylamine involving benzene derivatives have not been reported earlier. These results illustrate that, for phenylacetylene complexes, even minimal changes such as substitution by a methyl group, can result in change in the intermolecular structure. Here the underlying factors that influence the change in the intermolecular structure are discussed.

Methods

The details of the experimental set-up have been described elsewhere [7]. Briefly, helium buffer gas at 4 atm was bubbled through phenylacetylene and the requisite solvent kept at room temperature, and expanded through a 0.5 mm diameter pulsed nozzle. The LIF and 1C-R2PI spectra were recorded following electronic excitation monitoring either total fluorescence or the appropriate mass signal with time-of-flight mass spectrometer. The IR spectra were obtained using wither fluorescence dip infrared (FDIR) or ion dip infrared (IDIR) spectroscopic methods [8].

On theoretical front, geometry optimizations were carried out at MP2(FC)/aug-cc-pVDZ level of theory and in each case frequency

calculations followed to ascertain the nature of the minima obtained. Single point calculations at CCSD(T)/aug-cc-pVDZ level were carried out on the MP2 level optimized structures. The stabilization energies were corrected for zero point energy (ZPE) and basis set superposition error (BSSE). Thermochemical analysis, based on rigid rotor – harmonic oscillator – ideal gas approximations was also carried out using the vibrational frequency data obtained at MP2(FC)/ aug-cc-pVDZ level of theory. Further, DFT-SAPT (Symmetry Adapted Perturbation Theory) calculations were performed with aug-cc-pVDZ basis set [9], to separate of interaction energies into physically well defined components, such as those arising from electrostatic, induction, dispersion and exchange. The DFT-SAPT interaction energy (E^{int}) is given as

$$E^{int} = E_1^{Pol} + E_1^{Ex} + E_2^{Ind} + E_2^{Ex\text{-}Ind} + E_2^{D} + E_2^{Ex\text{-}D} + \delta HF$$

The above equation describes the electrostatic, exchange-repulsion, induction, exchange-induction, dispersion and exchange-dispersion terms, while the last term is a Hartree-Fock correction for higher-order contributions to the interaction energy. All calculations mentioned above were performed using Gaussian-03 and Molpro suit of programs [10,11].

Results and Discussion

The IR spectra of phenylacetylene (PHA) and its complexes with argon (Ar), water (H_2O), methanol (MeOH), ammonia (NH_3), and methylamine ($MeNH_2$) are presented in Figure 1. The IR spectrum of PHA (Fig. 1A) shows the presence of two strong transitions at 3325 and 3343 cm^{-1}, which were assigned to be originating due to Fermi resonance coupling between the acetylenic C–H stretching vibration and a combination band of comprising of one quantum of C≡C stretching and two quanta of C≡C–H out-of-plane bend [12]. Other weaker transitions were assigned to be originating from higher order coupling terms [12]. A two state de-perturbation analysis places the unperturbed acetylenic C–H oscillator at 3334 cm^{-1} with the magnitude of coupling constant to be 9 cm^{-1} [7]. In the case of PHA complexes any interaction that will perturb either the acetylenic

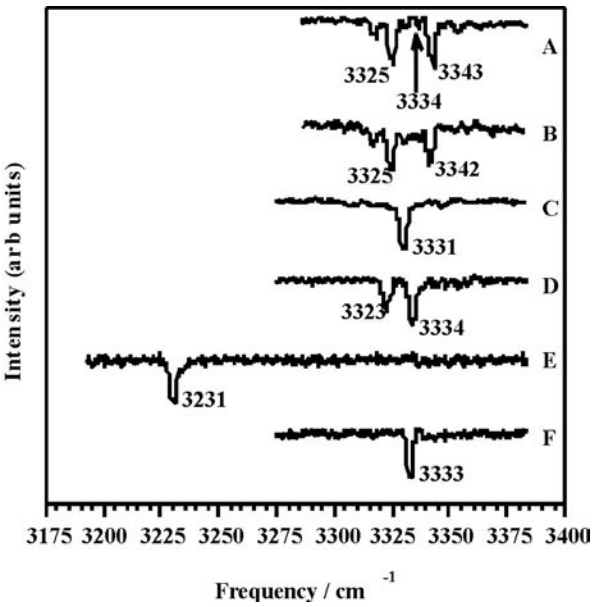

Figure 1 **:** *FDIR spectrum of (A) PHA, (B) PHA-Ar, (C) PHA-H_2O, (D) PHA-MeOH, (E) PHA-NH_3 and (F) PHA-$MeNH_2$, in the acetylenic C–H stretching region. The arrow indicates the position of the unperturbed C–H oscillator of PHA evaluated using two state de-perturbation model.*

C–H oscillator or the C≡C oscillator or both will lead to disappearance of Fermi coupling. However, the perturbation should be about the order of the coupling constant of 9 cm^{-1} or more, in order completely remove the Fermi mixing. The Fermi resonance transitions of PHA moiety, therefore, can be used a spectroscopic tool to probe the interactions present in various PHA complexes. The IR spectrum of Ar complex (Fig. 1B) is almost identical to that of bare PHA. This implies that the binding of Ar to PHA does not perturb either the C–H or the C≡C oscillators. It can therefore be inferred that Ar atom is bound to the π electron density of the benzene ring in PHA, in agreement with earlier reports [13,14].

The IR spectrum of H_2O complex (Fig. 1C) consists of a single transition at 3331 cm^{-1}. The spectrum of MeOH complex (Fig. 1D), on the other hand, shows (two transitions appear at 3323 and 3334 cm^{-1}. These spectra indicate that the interaction of water removes Fermi coupling while in the case of MeOH complex, the Fermi coupling is present, albeit some differences in the band positions and their intensities [6]. The difference in the nature of the IR spectra indicates that the mode of binding of H_2O and MeOH to

PHA are different. Further, the loss and presence of Fermi resonance coupling indicates that H_2O primarily interacts with the π electron density of the acetylenic **C**≡C bond, while MeOH primarily interacts with the π electron density of the benzene ring. In the case of NH_3 complex the IR spectrum (Fig. 1E) the acetylenic C–H stretching vibration shifts by 103 cm^{-1} to a lower frequency. Surprisingly, the IR spectrum of $MeNH_2$ complex (Fig. 1F) shows a single transition at 3333 cm^{-1}. It can be inferred from these spectra that NH_3 forms a C–H···N hydrogen-bonded, while $MeNH_2$ interacts with the π electron density of the acetylenic C≡C bond. The spectra in the acetylenic C–H stretching region suggest that the intermolecular structures of H_2O and MeOH are different, similarly the intermolecular structures of NH_3 and $MeNH_2$ are also different.

To understand the effect of methyl group substitution on the difference in the intermolecular structures of PHA complexes, high-level *ab-initio* calculations were carried out. Figure 2 depicts three minima found for the H_2O complex. Based on the IR spectrum in the acetylenic C–H stretching region along with the IR spectrum in the O H stretching region, the structure of the observed water complex can be assigned to **PW3** [4]. Similarly, in the case of MeOH complex, the observed structure can be assigned

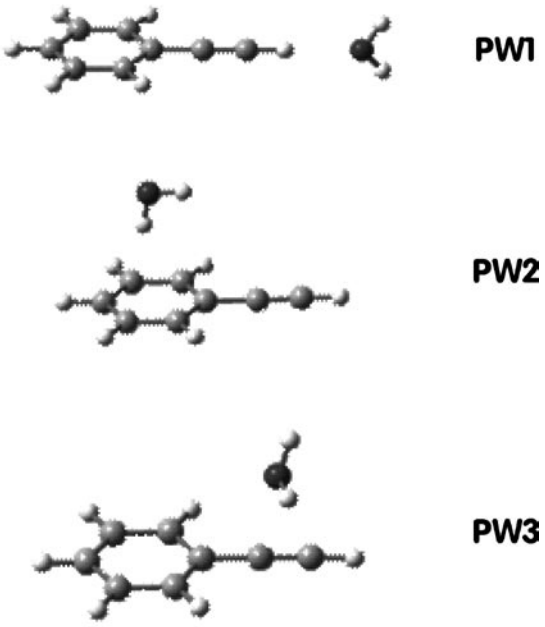

***Figure* 2 :** *Calculated structures of PHA-H_2O complex.*

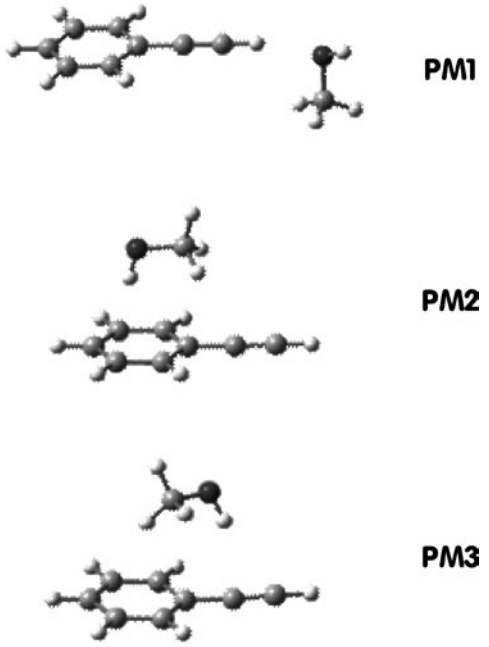

***Figure 3* :** *Calculated structures of PHA-H_2O complex.*

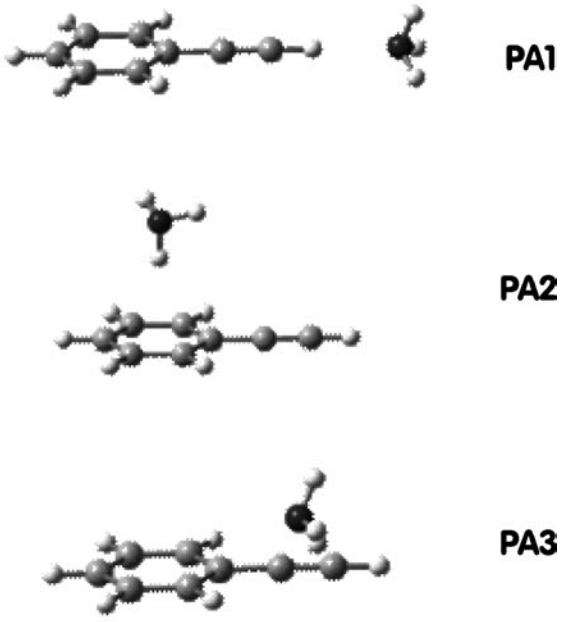

***Figure 4* :** *Calculated structures of PHA-NH_3 complex.*

to **PM2**, as shown in Figure 3 [6]. The calculated structures of NH_3 and $MeNH_2$ complexes are depicted in Figures 4 and 5, respectively. Once again base on the IR spectra in the acetylenic C–H stretching region, the observed structures of NH_3 and $MeNH_2$ complexes were assigned to **PA1** and **PMA2**, respectively [5]. Additionally, the above assignments were aided the other spectroscopic measurements, such as shifts in

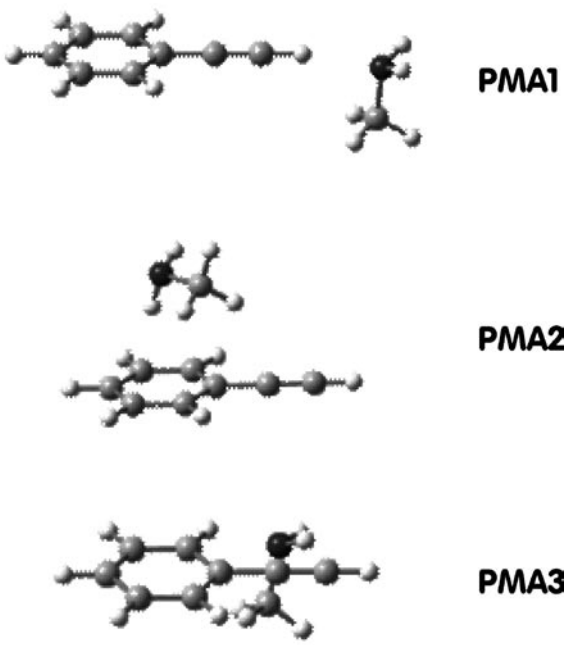

***Figure* 5:** *Calculated structures of PHA-$MeNH_2$ complex.*

TABLE 1: ZPE and BSSE Corrected Stabilization Energies (kJ mol^{-1}) of Various PHA Complexes Calculated using aug-cc-pVDZ Basis Set and ΔG for the Formation of Various Complexes at 10K.

	MP2	CCSD(T)	ΔG
PWS1	-6.4	-6.2	-5.6
PWS2	-8.1	-6.5	-6.3
PWS3	-7.6	-7.1	-7.0
PMS1	-9.8	-9.1	-8.3
PMS2	-13.6	-9.6	-8.7
PMS3	-13.1	-9.5	-8.3
PAS1	-8.7	-8.2	-8.3
PAS2	-5.4	-3.2	-2.8
PAS3	-6.7	-5.9	-5.6
PMAS1	-12.4	-11.3	-10.3
PMAS2	-10.6	-6.4	-5.6
PMAS3	-12.1	-9.4	-8.7

the electronic transitions and also the shifts in the O–H stretching frequencies for the H_2O and MeOH complexes [6].

The stabilization energies corrected for ZPE and BSSE for all the complexes are listed in Table 1. At MP2 level only the observed structures of MeOH (**PM2**) and NH_3 (**PA1**) complexes were found to be global minima, while the observed structures for PHA-H_2O (**PW3**) and PHA-$MeNH_2$ (**PMA2**) correspond to higher energy local minima. The MP2/aug-cc-pVDZ level is known to overestimate the dispersion energies, therefore single point calculations at CCSD(T) level were carried out. Table 1 also lists ZPE and BSSE corrected stabilization energies calculated at CCSD(T) level. At the CCSD(T) level the experimentally observed structure is the global minimum for the H_2O (**PW3**), MeOH (**PM2**) and NH_3 (**PA1**) complexes. The PHA-$MeNH_2$ complex (**PMA2**), however, is an exception and once again happens to be a higher energy (4.9 kJ mol^{-1}) local minimum.

The DFT-SAPT interaction energy decomposition was carried out for the all the structures. Table 2 lists the various components of the total energy and also the ZPE corrected SAPT stabilization energies. The ZPE corrected DFT-SAPT stabilization energies are comparable to the ZPE and BSSE corrected CCSD(T) energies. In the case of DFT-SATP calculations the observed complexes of H_2O (**PW3**) and NH_3 (**PA1**) are the global minima, while the complexes of MeOH (**PM2**) and $MeNH_2$ (**PMA2**) are higher energy local minima. For the PHA-H_2O system, the observed complex **PW3** has highest contribution in all the columns, which implies that this structure maximizes all the possible interactions. In the case of MeOH complex formation of observed **PM2** structure is favored by the dispersion contribution, while the electrostatic contribution is the lowest among the three isomers. In the case of NH_3 complex electrostatic and induction energies higher contributions for the observed **PA1** structure. On the other hand, dispersion energy has higher contribution in stabilizing the observed $MeNH_2$ complex, **PMA2**. A careful inspection of Table 2 reveals that electrostatics plays major role in stabilizing the observed structures of H_2O and NH_3 complexes, while dispersion plays a major role in stabilizing the observed structures of MeOH and $MeNH_2$. This implies that the substitution by methyl group switches the lead contribution from electrostatics to dispersion.

TABLE 2: DFT–SAPT Interaction Energy Decomposition (kJ mol^{-1}) for Various Complexes of PHA Calculated using aug-cc-pVDZ Basis Set

	E_{elec}	E_{ind}	E_{disp}	E_{exch}	δ_{HF}	E_{int}	E_{int} + ZPE
PW1	-17.0	-2.6	-6.4	17.4	-2.0	-10.6	-6.3
PW2	-11.9	-2.7	-13.1	18.2	-1.5	-11.0	-7.3
PW3	-25.5	-4.8	-13.6	32.2	-3.5	-15.2	-9.0
PM1	-20.9	-3.1	-10.2	24.8	-2.8	-12.2	-9.0
PM2	-17.4	-3.2	-26.1	36.2	-3.0	-13.5	-10.2
PM3	-20.2	-3.2	-25.6	37.7	-3.2	-14.6	-10.7
PA1	-24.9	-4.1	-8.4	27.0	-3.8	-14.2	-8.8
PA2	-9.3	-1.4	-14.4	19.1	-1.4	-7.4	-3.9
PA3	-22.4	-3.5	-13.8	29.8	-2.9	-12.8	-7.8
PMA1	-29.2	-4.7	-12.7	35.9	-5.2	-16.0	-11.8
PMA2	-15.4	-1.5	-26.3	35.2	-2.6	-10.6	-7.1
PMA3	-25.5	-3.3	-23.1	41.1	-3.6	-14.4	-10.8

Yet another parameter that was considered was the Gibbs free energy (G). This is due to the fact that the temperature of the experiment is non-zero, therefore the contribution of entropy cannot be neglected. The free energy surface includes the entropy contribution. The ΔG values were obtained by the thermochemical analysis following vibrational frequency calculations in Gaussian-03 at MP2/aug-cc-pVDZ level of theory and the electronic energy obtained at CCSD(T)/ aug-cc-pVDZ level. The ΔG for formation of all the complexes calculated at 10 K are also listed in Table 1. For H_2O, MeOH and NH_3 complexes the ΔG values at 10 K clearly indicate that the observed structures **PW2**, **PM2** and **PA1**, respectively are thermodynamically the most favored structures. While, in the case of $MeNH_2$ the observed **PMA2** is the least favored structure. The exclusive observation of **PMA2** structure in the present experimental conditions can therefore be attributed to the kinetic trapping.

In summary, the ability of formation of H_2O and NH_3 to form the thermodynamically most stable structures can be interpreted on the basis of dominance of electrostatic contribution to the total energy. On the other hand, for the MeOH and $MeNH_2$ complexes the higher polarizability of the O–H and N–H groups favor interaction with the π electron density of the benzene ring, wherein the dispersion forces dominate.

Acknowledgement

Author thanks his student Dr. Prashant Chandra Singh and collaborators Mr. Robert Sedlak and Prof. Pavel Hobza. Author also wishes to thank DST, BRNS and CSIR for the financial support.

References

1. M. C. Etter, Encoding and decoding hydrogen-bond patterns of organic compounds, *Acc. Chem. Res*. 23, 120-126 (1990).
2. C. Legon and D. J. Millen Angular geometries and other properties of hydrogen-bonded dimers: A simple electrostatic interpretation of the success of the electron-pair model, *Chem. Soc. Rev*. 16, 467-498 (1987).
3. The weak hydrogen bond by G. R. Desiraju and T. Steiner, Oxford University Press, Oxford, 2006.
4. P. C. Singh, B. Bandyopadhyay and G. N. Patwari, Structure of the Phenylacetylene-Water Complex as Revealed by Infrared-Ultraviolet Double Resonance Spectroscopy, *J. Phys. Chem.* A 112, 3360-3363 (2008).
5. P. C. Singh and G. N. Patwari, Electronic and vibrational spectroscopic investigation of phenylacetylene-amine complexes. Evidence for the diversity in the intermolecular structures, *J. Phys. Chem.* A 112, 4426-4431 (2008).
6. P. C. Singh and G. N. Patwari, IR-UV double resonance spectroscopic investigation of phenylacetylene-alcohol complexes. Alkyl group induced hydrogen bond switching, *J. Phys. Chem.* A 112, 5121-5125 (2008).
7. P. C. Singh and G. N. Patwari, Infrared-optical double resonance spectroscopy: A selective and sensitive tool to investigate structures of molecular clusters in the gas phase, *Curr. Sci*. 95, 469-474 (2008).
8. R. H. Page, Y. R. Shen and Y. T. Lee, Local modes of benzene and benzene dimer, studied by infrared-ultravoilet double resonance in a supersonic beam, *J. Chem. Phys*. 88, 4621-4636 (1988).

9. B. Jeziorski, R. Moszynski, K. Szalewicz, Perturbation Theory Approach to Intermolecular Potential Energy Surfaces of van der Waals Complexes, *Chem. Rev*. 94, 1887-1930 (1994).
10. J. Hasegawa, J. M. Ishida, T. Nakajima, et al., *Gaussian 03*, Revision A.1; Gaussian, Inc.: Wallingford, CT, 2003.
11. H. J. Werner and P. J. Knowles, MOLPRO, a package of *ab initio* programs designed by version 2006.1.
12. J. A. Stearns and T. S. Zwier, Infrared and ultraviolet spectroscopy of jet-cooled ortho-, meta-, and para-diethynylbenzene, *J. Phys. Chem*. A 107,10717-10724 (2003).
13. K. Siglow, H. J. Neusser, Rotationally resolved UV spectroscopy of weakly bound complexes: structure and van der Waals vibronic bands of phenylacetylene·*Ar*, *Chem. Phys. Lett*. 343, 475-478 (2001).
14. H. Dreizler, B. Hartke, H. D. Rudolph, A contribution to the structure of the van-der-Waals complex phenylacetylene–argon by microwave spectroscopy and quantum chemistry, *J. Mol. Struct*. 825, 1-19 (2006).

Prof. G. Naresh Patwari *received his Ph.D. in Chemical Sciences from Tata Institute of Fundamental Research in 2000. He was a JSPS postdoctoral fellow at Tohoku University, Sendai, JAPAN for two years (2000-2002) and also a Postdoctoral Fellow at the University of Illinois at Urbana-Champaign, USA for a year (2002-2003). He joined IIT, Bombay in 2003, where he is currently an associate professor. His current research interests include understanding of the intermolecular interactions at the fundamental level using a combination of experimental and theoretical methods, with specific applications to hydrogen storage materials, bio-conjugate chemistry, surface attachment of peptides and protein, and the effect of fluorination on the folding properties of proteins.*

Structures and Properties of Molecules and Clusters: Role of First-Principles based Computational Techniques

Tapan K Ghanty
Theoretical Chemistry Section, Chemistry Group, Bhabha Atomic Research Centre, Mumbai 400 085
E-mail: tapang@barc.gov.in

Abstract

First-principles based quantum chemical techniques can today be employed to determine the structures and properties of various molecular systems and also to predict the existence of new molecular species, which are hitherto not known. In this account we have described concisely some of our recent and ongoing work pertaining to the design of new molecular species involving rare gas atoms. The role of computational techniques in the calculation of excited state properties of molecular aggregates has also been discussed in brief.

I. Introduction

The role of computational chemistry is very broad and generally encompasses microscopic, mesoscopic and macroscopic systems. Here we confine ourselves to the domain of microscopic systems where quantum chemical techniques within the framework of molecular orbital theory or density functional theory are normally used. Computational quantum chemical methods are generally employed to calculate various physico-chemical properties such as molecular geometry in ground and excited states, charge and spin density distributions, potential energy surfaces, spectroscopic parameters, reaction rate constants, thermodynamic parameters, details of the dynamics of a process etc. In principle ab initio quantum chemistry [1] now allows the investigation of molecular species containing any atoms in the periodic table. It is possible mainly due to the availability of high-speed computers and efficient program packages based on recently developed algorithms. In particular, computational chemistry is highly useful in investigating potentially hazardous compounds that are difficult to handle in laboratory or inaccessible experimentally. Computational quantum chemical methods can also be employed for the prediction of the existence of novel chemical species. It can also be used in combination with experiment to corroborate or complement experimental results.

The underlying principles and the concerned quantum mechanical equations describing a many electron systems were known long back, however, solutions of those equations were not achieved successfully. Only in the fifties numerical solution of the Schrödinger equation for a many electron system has been possible [2] using the self-consistent-field theory of Hartree and Fock (HF) [3,4] within the framework of linear combination of atomic orbital (LCAO) approach. One major problem of HF theory is the missing of electron correlation term. Though the contribution of correlation energy to the total energy of a system is very small, it plays an important role in the prediction of physico-chemical properties of a chemical system. In subsequent years, with the formulation of density functional theory (DFT) [5] within an orbital-based framework by Hohenberg, Kohn and Sham [6,7], the electron correlation problem has been solved exactly, at least in principle. It has been demonstrated that electron density at all points in space is enough to uniquely determine the total energy of a system, and hence all of the other properties of the system. To accomplish this objective one has to assume a relationship between the total energy and the electron density function, which is popularly known as the "density functional". One component of this density functional, viz., exchange-correlation term is not known explicitly for a real system with inhomogeneous electron density distributions. Nevertheless, the corresponding

functional form for a homogeneous electron gas was known, which forms the basis of the local density approximation. Subsequently, several approximate exchange-correlation energy density functionals corresponding to inhomogeneous electron density distribution have been proposed within the framework of the homogeneous electron gas expression in the last two decades. In 1992, John Pople and his team have introduced DFT in the Gaussian program. Nowadays several such functionals are incorporated in all most all the standard quantum chemistry programs like GAMESS, Gaussian, Turbomole, ADF etc. Because DFT includes correlation energy, it is possible to obtain the structures and energies accurately with DFT methods. It is also important to note that computations using DFT is much less expensive as compared to that using other correlated methods based on Møller-Plesset perturbation theory, configuration interaction or multi-configuration approaches [1]. Thus, various chemical systems and processes can be modeled quite accurately using correlated quantum-chemical techniques for prediction and rationalization of experimentally observed results. In the following sections we discuss two specific areas, viz., (1) hydrogen-bonded systems (2) rare gas (noble gas) containing chemical compounds.

II. Hydrogen Bonding in the Excited State of Molecular Aggregates

Among the weak intermolecular interactions, hydrogen bonding has been the subject of increasing research activities [8-16] in recent years due to its importance in many chemical and biological systems and processes. Consequently, there have been a large number of theoretical and experimental investigations of several systems and processes involving hydrogen bonds. The strength of a hydrogen bond depends on the proton donating and proton accepting ability of the donor and the acceptor, respectively. The nature of bonding is mainly governed by the type of electronegative atom/group attached to the donor hydrogen atom, which affects the average position of bridging hydrogen atom (H_b) between the two electronegative atoms. The essence of the physical interactions that contribute to hydrogen bonding has been the subject of numerous discussions in the literature. In certain cases the type of interaction involved in the hydrogen bonding has been found to be bit controversial [17-18]

Water clusters system is one of the most important molecular aggregates where hydrogen bonding plays a central role. In recent years, water clusters have attracted considerable attention [19-24] from experimentalists as well as theoreticians. Representing a group of water molecules bonded through rather weak hydrogen bonds, water clusters play a unique role as one of the most important molecular clusters, forming a link between the isolated water molecules and bulk water. Significant amount of research work has been carried out on the investigation of the structural arrangement of the water molecules in water clusters, of particular importance being the dependence of the geometry and structural transition on the aggregation number n. However, much less attention has been paid towards the investigations of methanol clusters. There will be certain similarity as well as difference between the water and methanol clusters because of the presence of one methyl group in methanol in place of hydrogen in water. Therefore, it would be interesting to compare the properties of water and methanol clusters in both ground and excited states. It is to be noted that there have been several reports on the ground state properties on these clusters; however, excited state investigations on these molecular aggregates are scarce. Nevertheless, for the sake of completeness we will discuss both ground and excited state properties of these clusters.

Recently, investigation on the molecular systems in their excited states has received significant attention from various researchers [25-35]. Modeling of solvation process using QM/MM like approach has become quite popular in the recent past. One of the recent methods, viz., effective fragment potential approach, popularly known as EFP [34-35], to model solvent using atomic charges, molecular dipole moments, molecular polarizability etc. in the ground state has received considerable attention. Excited state solvent can also be modeled in a similar way

using corresponding excited state parameters. Modeling of excited state solvent by using excited state dipole moment and polarizability parameters may be quite important in the field of solvation dynamics and hydrogen-bond dynamics in the excited state, and in molecular dynamics simulation in the excited state. Polarizability values of hydrogen bonded clusters in the excited states might play an important role in modeling the excited state properties of the corresponding bulk liquid. In this context it is to be noted that the excited state properties of liquid water has been reviewed [32] recently.

In recent times, there have been several reports in the literature on the excited-state polarizability for a number of molecular systems. For instance, excited-state polarizabilities calculated using TDDFT method have been compared with the corresponding experimentally estimated values for various conjugated molecular systems[36-37] and porphyrin derivatives [38]. In general, excited-state polarizabilities are determined experimentally by flash photolysis time-resolved microwave conductivity techniques or electroabsorption/electroemission measurements (Stark shift spectroscopy) [39]. Changes in polarizability upon excitation contain valuable information on the nature of molecules in their electronically excited state, the so-called exciton state. Exciton polarizability in semiconductor nanocrystals determined using terahertz time-domain spectroscopy has also been reported recently [40]. Changes in average polarizability on electronic excitation of non-polar, polar and ionic compounds has been investigated [41] by using the spectral solvent-shift of absorption band maxima. Mechanism for the high enhancement of static polarizability in going from ground to excited states in porphyrin J-aggregates has been documented [42] in the literature. Excited state polarizabilities of solvated molecules have also been calculated [43] using both equilibrium and non-equilibrium solvation models. Thus, it is clearly evident that excited polraizabilities are of considerable recent interests. Therefore, we have been motivated to calculate the excited polaraizabilities of methanol clusters with an objective to investigate the variations of polarizabilities of the first two excited states of methanol clusters with the size of the clusters by using TDDFT.

Despite extensive literature on the structures and properties of water and methanol clusters, it is surprising that virtually no work has been reported on the excited state polarizabilities of the water and methanol clusters by using conventional electronic structure methods. The objective of this work is to investigate the static dipole polarizabilities, vertical excitation energies and oscillator strengths of the methanol clusters in the excited states using ab initio method within the framework of time dependent density functional theory (TDDFT). It is difficult and often even impossible to obtain reliable experimental data for these target properties due to various practical limitations. Therefore, we turn to TDDFT and generate the required reference data computationally. A number of investigations have been reported over the past several years to suggest that TDDFT is a powerful tool for the calculation of electronic excited states [44-49], particularly for valence like transitions. The static electric dipole polarizability is a measure of the distortion of the electron density under the effect of an external static electric field. At the same time, an excited state may be considered as a perturbed ground state as far as the electron density distribution is concerned. Thus, two different kinds of perturbations are involved in the calculation of polarizability for an excited state of a molecule. Therefore, it is interesting to investigate [50] the variation of excited states polarizabilities of clusters with the cluster size (n), particularly for hydrogen-bonded water and methanol clusters.

The calculated first excited state as well as the second excited state polarizabilities are found [50] to increase with the aggregation number of methanol clusters, although, in one or two cases, the trend is not monotonic. Therefore, in Figure 1, we have plotted the polarizability values corresponding to the first excited state against the aggregation number n. Polarizability values corresponding to the second excited state have also been plotted against the aggregation number n in Figure 2. The first and second

excited states polarizabilities have good linear correlation (correlation coefficient ~ 0.97-0.98) with the aggregation number of methanol

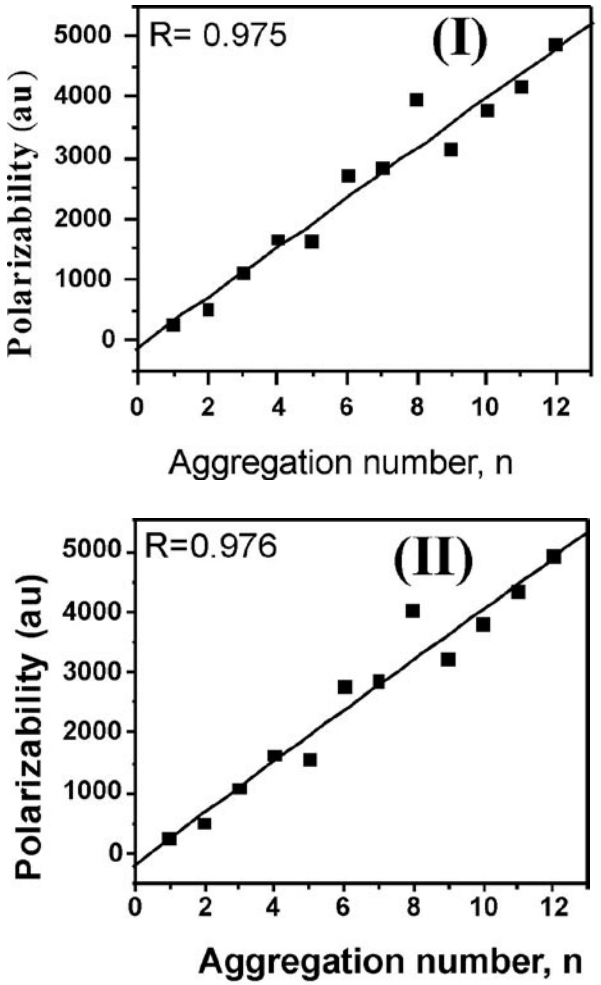

Figure 1 : *First excited state polarizabilities as a function of aggregation number (n) of methanol clusters. The calculated results are based on the TDDFT/B3LYP method and (I) Sadlej basis set and (II) 6-311++G (d,p) basis set. The 'R' in the figures indicate correlation coefficient corresponding to the linear fit of polarizability with cluster size, n.*

clusters (Figures. 1-2). The correlation coefficients corresponding to different basis sets and excited states are shown in respective Figures.

Recently, it is reported [51] that the ground state polarizabilities vary linearly as a function of the size of the methanol clusters with a correlation coefficient of ~1. Earlier, Ghanty and Ghosh have also reported [52] similar trend of variation of polarizabilities with size for water clusters in the ground state (Figure 3). However, here, the correlation of polarizability with aggregation

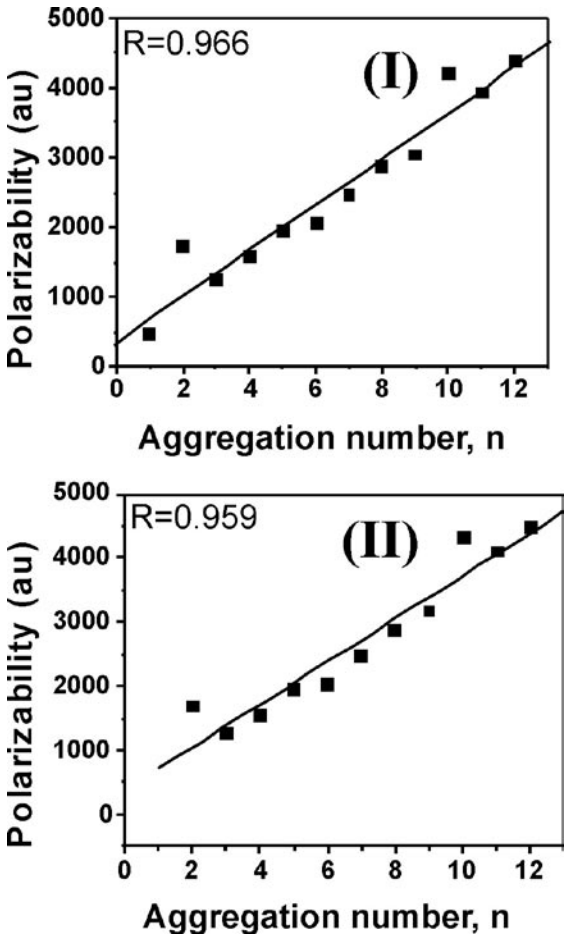

Figure 2 : *Second excited state polarizabilities as a function of aggregation number (n) of methanol clusters. The calculated results are based on the TDDFT/B3LYP method and (I) Sadlej basis set and (II) 6-311++G (d,p) basis set. The 'R' in the figures indicate correlation coefficient corresponding to the linear fit of polarizability with cluster size, n.*

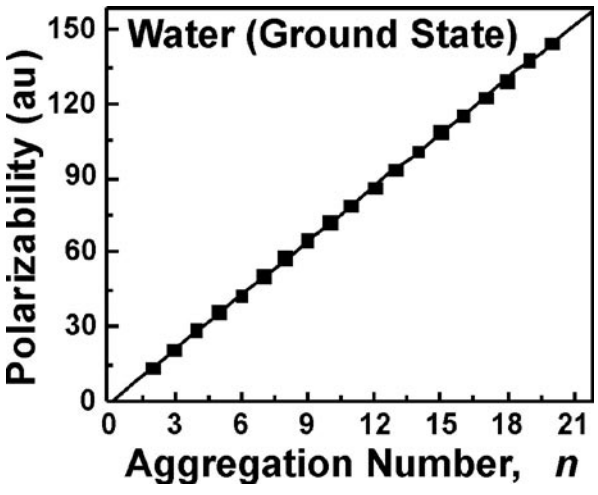

Figure 3 : *Ground State Polarizabilities of Water Clusters as a function of aggregation number (n).*

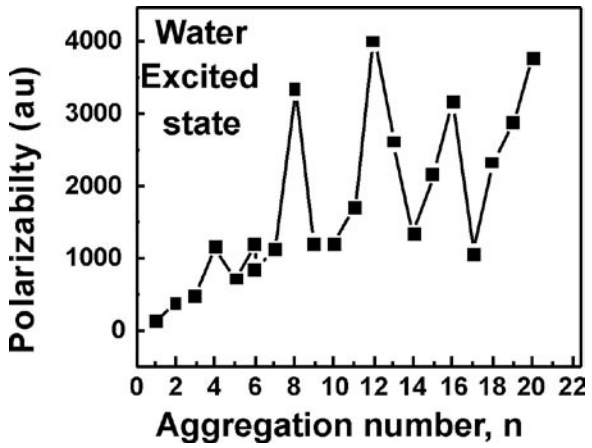

Figure 4 : *First excited state polarizabilities as a function of aggregation number (n) of water clusters. The calculated results are based on the TDDFT/B3LYP method and 6-311++G (d,p) basis set.*

number is demonstrated in the electronic excited states for the first time [50] for methanol clusters. Motivated by this, we have also calculated the polarizabilities of the water clusters in their excited states and the results for the first excited state are plotted in Figure 4. It is clear that the first excited state polarizability values vary in a rather non-monotonic fashion with respect to the cluster size. In fact we have attempted to find a correlation between the excited state polarizabilities of water clusters with the cluster size up to n=12, and found that the correlation corresponding to a linear least square fit is very poor with a correlation coefficient of only 0.732. Similarly, for metal clusters, the polarizability values vary with the size of the cluster [53-57] in a rather zigzag fashion. Thus, it is evident that this sort of correlation for the excited states exists for the methanol clusters and not for water clusters. Investigation on more systems might be essential for arriving at any general conclusion in this matter.

The singlet excitation energies corresponding to the first, second and third excited states are also plotted as a function of the aggregation number of methanol clusters for different basis sets (Figure 5). The excitation energies and oscillator strengths are found to decrease as a function of n and converge to the bulk value very soon. The electronic excitation energies are found to be lower for cluster with n=2. The effect of basis

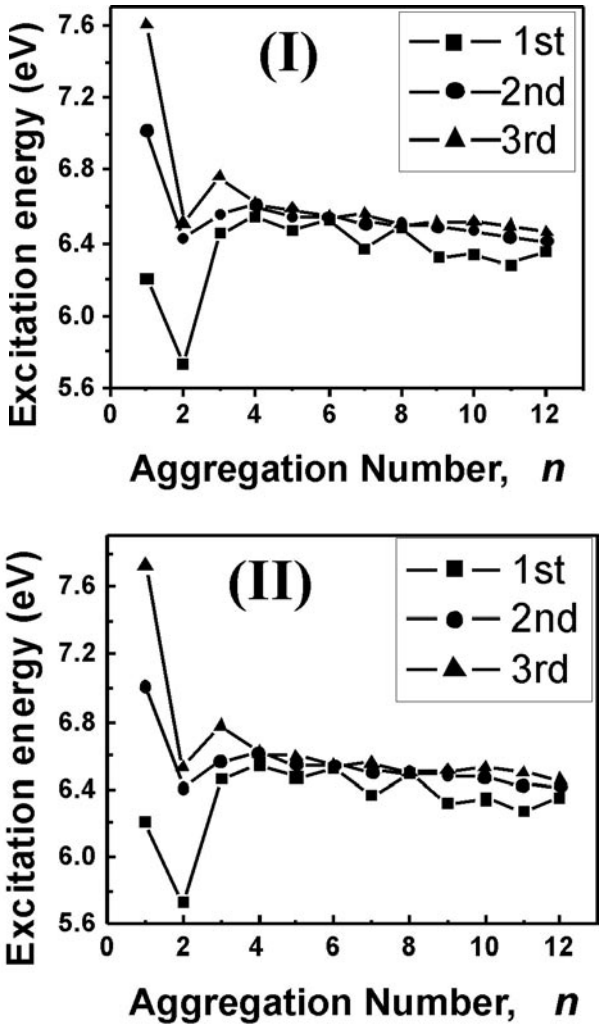

Figure 5 : *Variation of excitation energies as a function of aggregation number (n) of methanol clusters. The calculated results are based on the TDDFT/B3LYP method and (I) Sadlej basis set and (II) 6-311++G (d,p) basis set.*

sets on the calculated excitation energies is found to be negligible. Similarly, for the water clusters we have plotted the excitation energies in Figure 6. In general, excitation energies for the water clusters are higher than the corresponding values for the methanol clusters. From Figures 5 and 6 it is clear that the variation in excitation energy with cluster size for the water clusters is higher as compared to the same for methanol clusters. In fact, for the water clusters (up to n=20), the excitation energy for n=15 is found to be smaller than that for n=2 for all the three excited states. Also, for n=7 and n=11, the polarizability values for the first excited state are rather smaller than that for the neighboring clusters.

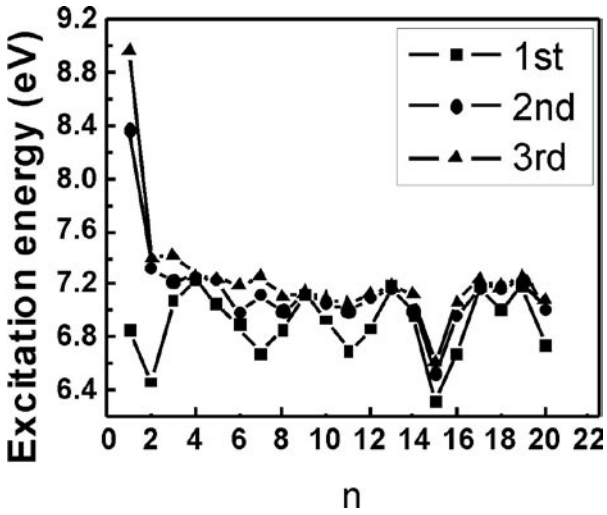

Figure 6 : *Variation of excitation energies as a function of aggregation number (n) of water clusters. The calculated results are based on the TDDFT/B3LYP method and 6-311++G (d,p) basis set.*

We have attempted to analyze the variations of excited state polarizabilities of water and methanol clusters. We have observed that the variation of excitation energy from one cluster size to another for water cluster is much higher as compared to that in the methanol clusters. This trend indicates that perturbation due to excitation for water cluster is significantly higher than that in methanol cluster. Consequently, perturbation due to electric field, which in turn dictates the variation of polarizability from one water cluster to another cluster, is strongly influenced by the excitation process. That may be the reason for non-monotonic variation of water cluster polarizabilities in the excited states. We have also observed that whenever the HOMO-LUMO gap of a particular water cluster is higher than its neighboring clusters, excited state polarizability for that particular cluster is considerably larger. For example the HOMO-LUMO gaps for n=7 to 9 have been found to be 0.2788, 0.2894 and 0.2814 a.u., respectively. Since a larger HOMO-LUMO gap of a particular cluster (here n=8) is associated with greater stability of that cluster in the ground state, more energy is required to excite that cluster in the excited state. Therefore, it is quite clear that the excited state for n=8 cluster is likely to be more polarizable. Similar trend is observed for the n=12 cluster. Again, this trend is consistent with the variation of excitation energy from one cluster size to another cluster in water cluster.

Therefore, electron density distributions in the excited states of water clusters are expected to vary with size in a quite different manner as compared to the same in methanol clusters. This is clearly due to the difference in the nature of hydrogen bonds in the two sets of clusters. This aspect has been discussed recently by Krishtal et al [51] in the context of variation of ground state polarizability of methanol clusters with size. It has been emphasized that the presence of a hydrophobic methyl group and only one hydrophilic hydroxyl group in a methanol molecule, in contrast to the presence of two hydrophilic hydroxyl groups in a water molecule results in difference in the nature of the hydrogen bonds in water and methanol clusters. Accordingly, the dependence of polarizability on the hydrogen bond network in a water cluster is expected to be different from that in a methanol cluster. Apart from the hydrophobic nature of the methyl group, steric effect arising due to the presence of hydrophobic methyl group is also likely to contribute to the difference in the calculated polarizability of methanol clusters as compared to the water clusters. Also, the extent of intermolecular charge transfer in a water cluster is higher than that in methanol cluster. All these factors are responsible for the linear and non-linear variation of polarizability with cluster size for methanol and water clusters, respectively.

III. Prediction of Novel Rare gas Molecules

In recent years there has been an upsurge of interest in the investigation on the existence of rare gas compounds. It is well known that the noble gas elements helium, neon, argon, krypton, and xenon are chemically inert due to their closed shell octet configurations in the ground state. Nevertheless, search for the rare-gas compounds has been initiated since Pauling's prediction [58] on the possibility of chemical bonding of heavier rare-gas elements due to the less shielding effect of the outer valence electrons from the nucleus. This prediction has been realized in 1962 by Bartlet [59] through the synthesis of the first rare-gas compound, xenon hexafluro-platinate $[Xe^{+}(PtF_6)^{-}]$. The synthesis of the first noble gas compound proves one of the the unusual

examples of chemical bonding; therefore their exploration unravels new bonding mechanism and expands our understanding of a chemical bond. In recent years, several novel rare-gas compounds have been predicted theoretically as well as prepared and identified experimentally [60]. Among them the most notable development has been the preparation and characterization of the HNgX species using matrix isolation technique by Räsänen and co-workers [61] where Ng is a rare-gas atom such as Ar, Kr, and Xe, and X is an electronegative atom or group. In the recent past, Seidel and Seppelt reported [62] the existence of first bulk compound, $AuXe_4^{2+}$ $[Sb_2F_{11}^-]_2$ containing a noble gas-noble metal bond (Au-Xe). It is in sharp contrast to the conventional inert behavior of noble gas and noble metal atoms that have nearly covalent bonds between gold and xenon. Here it is important to note that noble metal such as gold has a very rich and unusual chemistry due to the strong relativistic effects resulting in this kind of unusual behavior [63,64].

Here we consider [65] altogether a new class of rare gas compounds containing noble gas-noble metal bond where a noble gas atom (Ng) is inserted into a noble metal molecule (AuX) resulting into the formation of Au-Ng-X species. Essentially, the hydrogen atom in H-Ng-X has been replaced by a gold atom to form Au-Ng-X species. The origin of this development has been the hydrogen-like chemical behaviour of a gold atom in various gold compounds [66,67]. In the spirit of this behavior of a gold atom as a hydrogen atom we have investigated [65] the bonding between a noble gas atom and a noble metal atom in the insertion compounds Au-Ng-X (Ng=noble gas atom and X= electronegative atom or group), e.g. AuKrF and AuXeF. Again, we have also considered the possibility [68] of a chemical bond between other coinage metal atoms, viz., Cu and Ag, and rare gas atoms. Thus, here our objective has been to investigate the structure and properties of the M-Ng-F compounds with the aid of quantum chemical calculations and to explore whether they are stable or not with reference to their corresponding dissociated products on the respective potential energy surface.

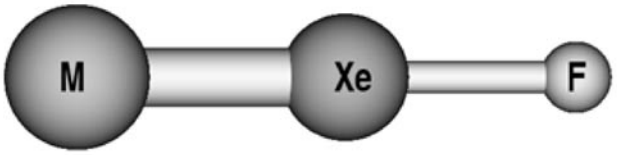

CuXeF	2.411	2.280
AgXeF	2.651	2.291
AuXeF	2.585	2.140

Figure 7: *Structure of the optimized MXeF (M=Cu, Ag and Au) molecules.*

The optimized structures of the MXeF species (M=Cu, Ag and Au) shown in Figure 7 reveal that they are linear. The Cu-Ng bond lengths in CuArF, CuKrF and CuXeF have been found to be 2.161 Å, 2.253 Å and 2.451 Å, respectively. A similar trend is observed in the Ag compounds, where the calculated Ag-Ng bond lengths are 2.433 Å, 2.506 Å and 2.651 Å for AgArF, AgKrF and AgXeF, respectively. It is interesting to compare the noble metal-noble gas bond lengths as obtained in the present work with that of earlier reports for different class of noble-gas compounds, viz., NgMF [69,70] containing noble metal-noble gas bonding. A detail comparison reveals that the present calculated M-Ng bond length in MNgF species are always smaller than that in NgMF systems published in the literature [69,70] (also calculated here for the sake of consistency in methods, basis sets etc.). It is interesting to note that the deviations in the M-Ng bond lengths in the two classes of compounds, viz., MNgF and NgMF are more for the Cu-Ar, Ag-Ar and Ag-Kr bonds, and the respective differences are 0.071, 0.181 and 0.103 Å. However, for the Au-Ng bond the two sets of values are found to be almost the same. It indicates that the M-Ng bonds in MNgF (with M=Cu and Ag, and Ng=Ar and Kr) are relatively shorter than that in NgMF as compared to the Au-Ng bonds in the two classes of species. As a consequence, the M-Ng interaction in MNgF species is likely to be stronger than that in NgMF systems. Also, the larger Ng-F bond length in CuNgF and AgNgF as compared to that in AuNgF indicates that the Ng atom interacts rather weakly with F atom in CuNgF and AgNgF. As a result, the Cu-Ng or Ag-Ng interaction is

again expected to be stronger. In view of the interesting reports [69,70] on comparison of the M-Ng bond length with respect to a covalent limit, R_{cov} [r_{cov} (M(I) + r_{cov} (Ng)] and a van der Waals limit, R_{vdw} [r_{ion} (M^+) + r_{vdw} (Ng)] we have compared and found that the calculated M-Ng bond lengths in MNgF species are much closer to the covalent limit as compared to the van der Waals limit. In fact, it is important to note that the Cu-Kr bond length in CuKrF is slightly smaller than the corresponding covalent limit. Also, the difference between the calculated Cu-Xe bond length and the corresponding covalent limit is merely 0.041 Å. All these results are somewhat in contrast to the earlier reports [14,15] involving NgMF species where it has been observed that for the Ar compounds the Ar-Ng bond lengths are closer to the van der Waals limit and Kr-Ng bond lengths are in between the two limits. The calculated bond length values also indicate that the Au-Xe bond is closer to the covalent limit as compared to the van der Waals limit. On the other hand, for $[AuXe_4]^{2+}$ the Au-Xe bond distance is rather large (2.79 Å) and lies in between covalent and van der Waals limit. Now it is interesting to compare the M-Ng bond lengths in MNgF species with the sum of triple bond covalent radii proposed recently [71]. For the AgNgF species the Ag-Ng bond distances are slightly above the corresponding triple bond covalent radii sum. However, the Cu-Ng bond distances in CuNgF species are very close to the respective covalent radii sum. In fact, it is important to note that the Cu-Kr bond length in CuKrF is smaller than the sum of triple bond covalent radii, implying a partial triple bond nature in the noble metal atom and the noble gas atom bonding.

It is important to note that some of the calculated values of the M-Ng bond dissociation energies (with Ng=Kr and Xe) are remarkably larger in MNgF species than that in NgMF systems. For instance, the Cu-Xe bond energy in CuXeF (139.1 kJ/mol) is ~2 times (~105%) larger than the same in XeCuF (67.9 kJ/mol) species. Similarly, the Ag-Xe bond energy in AgXeF (101.1 kJ/mol) is ~2.7 times (165%) larger than the same in XeAgF (38.1 kJ/mol) species. The calculated value of Au-Xe bond energy in AuXeF molecule (109.8 kJ/mol) has been found to compare very well with previous Au-Xe bond energy obtained for other compounds, viz. XeAuF (101.0 kJ/mol), $XeAu^+$ (127.0 kJ/mol) and $XeAuXe^+$ (108.0 kJ/mol). It is also interesting to compare the variation of the M-Ng bond energy along the series Cu-Ag-Au for the two sets of species, viz., MNgF and NgMF. Considering the present calculated values it has been found that the M-Ng bond energies in MNgF species (with Ng=Kr and Xe) follow the trend, Cu-Ng>Ag-Ng≥Au-Ng, which is somewhat different than that observed in NgMF species (Au-Ng>Cu-Ng>Ag-Ng) [69,70]. In this context it is important to note that the Au-Xe bonding has been predicted theoretically before its existence has been established experimentally. To assess the stability of the predicted noble gas compounds further, we have calculated the energies corresponding to the various dissociated products of MNgF molecules. It has been found that AuKrF and AuXeF are less stable than AuF + Kr and AuF + Xe by 276.0 and 166.2 kJ/mol, respectively at the MP2 level of theory. An alternative channel to decompose MNgF is a direct dissociation of M-Ng and Ng-F bonds leading to the formation of M + Ng + F. The dissociation energies corresponding to this channel indicate that most of these species are metastable and have a local minimum in their respective potential energy surfaces. The kinetic stability of the MNgF species have been assessed through calculations of the transition state corresponding to the MF + Ng dissociation channel. The calculated barrier heights corresponding to the respective transition states indicate that most of the species should be kinetically stable with respect to the bending reaction coordinate. Apart from the prediction of noble metal – noble gas bonding, we have also envisaged few other noble gas containing chemically bonded species, viz., HXeOH, HBeNgF, FBeNgF, FMgNRgF, $FXeBF_2$, $HNgCO^+$ [72-76].

IV. Concluding Remarks

In this article, the potential role of computational chemistry in the prediction and rationalization of structure and properties of two different types of chemical systems have been discussed briefly. The investigation of noble

gas compounds proves the unusual examples of chemical bonding; therefore their exploration unravels new bonding mechanism and expands our understanding of a chemical bond. We have also discussed the computed results on the ground and excited states polarizabilities of the water and methanol clusters, and the difference in the trend in the excited state polarizabilities of water and methanol clusters has been attributed to the dissimilarity in the nature of hydrogen bonding in the two sets of clusters due to the presence of $-CH_3$ group in methanol. Demonstration of an excellent linear correlation between the ground state polarizability of water clusters and the aggregation number may be very useful to obtain the polarizability of larger cluster from the cluster size. All the work discussed here demonstrates the predictive ability of first-principles based computational techniques.

Acknowledgments

I am extremely grateful to Dr. Swapan K. Ghosh, Head, Theoretical Chemistry section for his excellent guidance, help and support since the beginning of my research carrier at BARC. I am very much thankful to my collaborators, Dr. G. B. Dutt, Dr. R. Joshi and Dr. D. K. Palit, Radiation & Photochemsitry Division, BARC, Dr. T. Jayasekharan, Applied Spectroscopy Division, BARC and Dr. K. Gupta, Ramananda College, Bishnupur for many helpful discussions. It is a pleasure to thank Dr. Tulsi Mukherjee, Director Chemistry Group for his kind interest, help and constant encouragement. Computer Division, BARC, is gratefully acknowledged for providing computational facilities and support.

References

1. (a) W. J. Hehre, L. Radom, P. v. R. Schleyer and J. A. Pople, "Ab Initio Molecular Orbital Theory", John Wiley & Sons, New York, 1986; (b) F. Jensen, *Introduction to Computational Chemistry, Wiley, Chichester, (1999).*
2. *C. C. J. Roothaan, Rev. Mod. Phys.* **1960**, *32, 179.*
3. D. R. Hartree, The Calculation of Atomic Structures, Chapman and Hall, London (1957).
4. *V. Fock, Z. Phys* **1930**, *61, 126.*
5. R. G. Parr and W. Yang, Density Functional Theory of Atoms and Molecules , Oxford University Press: New York, (1989).
6. P. Hohenberg and W. Kohn, *Phys. Rev.* **1964**, *B136, 864.*
7. W. Kohn and L. Sham, *Phys. Rev.* **1965**, *A140*, 1133.
8. G. A. Jeffrey and W. Saenger *Hydrogen Bonding in Biological Structures*; Springer: Berlin, 1991; G. A. Jeffrey, *An Introduction to Hydrogen Bonding*; Oxford University Press: New York, 1997.
9. S. Scheiner, *Annu. Rev. Phys. Chem.* **1994**, *45*, 23; S. Scheiner, *Hydrogen Bonding: A Theoretical Perspective*; Oxford University Press: New York, 1997.
10. M. S. Gordon and J. H. Jensen, *Acc. Chem. Res.* **1996**, *29*, 536.
11. I. Alkorta, I. Rozas and J. Elguero, *Chem. Soc. Rev.* **1998**, *27*, 163.
12. T. K. and Ghanty and S. K. Ghosh, *J. Phys. Chem.* A **2002**, *106*, 4200; *J. Phys. Chem.* A **106** 11815 (2002); *J. Phys. Chem.* A **107 7062 (2003).**
13. L. Senthilkumar, T. K. Ghanty, and S. K. Ghosh**,** *J. Phys. Chem. A* **2005**, *109,* 7575; L. Senthilkumar, T. K. Ghanty, S. K. Ghosh and P. Kolandaivel, *J. Phys. Chem. A* **2006**, *110, 12623.*
14. *A. Bhattacharyya, P. K. Mohapatra, T. K. Ghanty and V. K. Manchanda, Phys. Chem. Chem. Phys.* **2008**, *10, 6274.*
15. *R. Joshi, T. K. Ghanty, S. Naumov and T. Mukherjee, J. Phys. Chem. A* **2007**, *111, 2362.*
16. *R. Joshi, T. K. Ghanty, S. Naumov and T. Mukherjee, J. Phys. Chem. A* **2007**, *111,* 13590; R. Joshi, T. K. Ghanty, S. Naumov and T. Mukherjee, *Chem. Phys. Lett.* **2009**, *471*, 36.
17. E. D. Isaacs, A. Shukla, P. M. Platzman, D. R. Hamann, B. Barbiellini, C. A. Tulk, *Phys. Rev. Lett.* **1999**, *82*, 600.
18. T. K. Ghanty, V. N. Staroverov, P. R. Koren and E. R. Davidson, *J. Am. Chem. Soc.* **2000**, *122* , 1210.
19. R. Ludwig, *Angew. Chem. Int. Ed.* **2001** *40*, 1808.
20. R. Ludwig, *ChemPhysChem* **2000** *1*, 53.
21. J. K. Gregory, D. C. Clary, K. Liu, M. G. Brown, R. J. Saykally, *Science* **1997,** *275*, 814.
22. M. Henry, *ChemPhysChem* **2002,** *3*, 101.
23. S. S. Xantheas, Editor, *Recent Theoretical and Experimental Advances in Hydrogen Bonded Clusters*, Kluwer, Dordrecht (2000).
24. S. Maheswary, N. Patel, N. Sathyamurthy, A. D. Kulkarni and S. R. Gadre, *J. Phys. Chem.* **A 2001,** *105, 10525.*
25. *D. K. Palit, T. Zhang, S. Kumazaki and K. Yoshihara, J. Phys. Chem. A* **2003**, *107, 10798.*
26. *V. Samant, A. K. Singh, G. Ramakrishna, H. N. Ghosh, T. K. Ghanty, and D. K. Palit, J. Phys. Chem. A* **2005**, *109*, 8693; J.A. Mandal, V. Samant, M. Varne, A.K. Singh, T.K. Ghanty, H.N. Ghosh and D. K. Palit, *Chem.Phys.Chem.* **2009**, *10, 2995.*
27. *G. B. Dutt and T. K. Ghanty, J. Chem. Phys.* **2003**, *119*, 4768; G.B. Dutt and T.K. Ghanty, *J. Chem. Phys.* **2003**, *118*, 4127; G. B. Dutt and T. K. Ghanty, *J. Phys. Chem.* A **2004**, *108*, 6090; G. B. Dutt, *ChemPhysChem*. **2005**, *6, 413.*
28. *N. P. Wells, M. J. McGrath, J. I. Siepmann, D. F. Underwood and D. A. Blank, J. Phys. Chem. A* **2008**, *112,* 2511; S. J. Schmidtke, D. F. Underwood and D. A. Blank, *J. Phys. Chem. A* **2005**, *109,* 7033.
29. C. G. Elles, I. A. Shkrob, R. A. Crowell, and S. E. Bradforth, *J. Chem. Phys.* **2007**, *126, 164503.*
30. *S. Tretiak, A. Saxena, R. L. Martin, and A. R. Bishop. Proc. Natl. Acad. Sci* (USA), **2003**, *100, 2185.*
31. M. Odelius, H. Ogasawara, D. Nordlund, O. Fuchs, L. Weinhardt, F. Maier, E. Umbach, C. Heske, Y. Zubavichus, M. Grunze, J. D. Denlinger, L.G. M. Pettersson and A. Nilsson, *Phys. Rev. Lett.* **2005**, *94*, 227401; M. Odelius, *Phys. Rev. B* **2009**, *79, 144204.*
32. V. Garbuio, M. Cascella and O. Pulci, *J. Phys.: Condens. Matter* **2009**, *21, 033101.*
33. O. T. Ehrler and D. M. Neumark, Acc. *Chem. Res.* **2009**, *42, 769*

34. D. Kina, A. Nakayama, T. Noro, T. Taketsugu and M. S. Gordon, *J. Phys. Chem. A* **2008**, *112*, 9675.
35. H. Li, H. M. Netzloff, and M. S. Gordon, *J. Chem. Phys.* **2006**, *125, 194103.*
36. *F. C. Grozema, R. Telesca, H. T. Jonkman, L. D. A. Siebbeles and J. G. Snijders, J. Chem. Phys.*, **2001**, *115*, 10014.
37. F. C. Grozema, R. Telesca, J. G. Snijders and L. D. A. Siebbeles, *J. Chem. Phys.*, **2003**, *118*, 9441.
38. G. H. Gelinck, J. J. Piet, B. R. Wegewijs, K. Müllen, J. Wildeman, G. Hadziioannou and J. M. Warman, *Phys. Rev. B* **2000**, *62, 1489.*
39. F. Wang , J. Shan, I. A. Mohammad, I. P. Herman, M. Bonn and T. F. Heinz, *Nature Materials, 2006, 5, 861.*
40. R. Improta, C. Ferrante, R. Bozio and V. Barone, *Phys. Chem. Chem. Phys.*, **2009**, *11, 4664.*
41. I. Renge, *Chem. Phys.* **1992**, *167*, 173; *Chem. Phys. Lett.* **2008**, *459, 124.*
42. T. Katsumata, K. Nakata, T. Ogawa, K. Koike, T. Kobayashi and E. Tokunaga, *Chem. Phys. Lett.* **2009**, *477, 150.*
43. K. Ruud, B. Mennucci, R. Cammi and L. Frediani, J. Comput. Methods in Sciences and Engineering, **2004**, *4, 381.*
44. C. Adamo and V. Barone, *J. Chem. Phys.* **1998**, *108, 664* .
45. C. Adamo and V. Barone, *Chem. Phys. Lett.* **1999**, *314, 152* .
46. C. Adamo , G. E. Scuseria, and V. Barone, *J. Chem. Phys.* **1999**, *119, 2889.*
47. C. Adamo and V. Barone, *Chem. Phys. Lett.* **2000**, *330, 152* .
48. R. J. Cave and E. W. Castner, Jr., *J. Phys. Chem.* A **2002**, **106, 9294 .**
49. D. Jacquemin, E. A. Perpéte, G. E. Scuseria, I. Ciofini and C. Adamo, *J. Chem. Theor. Comput.* **2008**, *4, 123.*
50. K. Gupta, T. K. Ghanty and S. K.; Ghosh, *Phys. Chem. Chem. Phys* **2010**, *12, 2929.*
51. A. Krishtal, P. Senet and C. V. Alsenoy, *J. Chem. Theory Comput.* **2008**, *4, 426.*
52. T. K. Ghanty and S. K. Ghosh, *J. Chem. Phys.* **2003**, *118, 8547.*
53. K. R. S Chandrakumar, T. K. Ghanty and S. K. Ghosh, *J. Phys. Chem.* A **2004**, *108, 6661.*
54. K. R. S Chandrakumar, T. K. Ghanty and S. K. Ghosh, *J. Chem. Phys.* **2004**, *120*, 6487.
55. A. Banerjee, A.Chakrabarti and T. K. Ghanty, *J. Chem. Phys* **2007**, *127*, 134103; A. Banerjee, T. K. Ghanty, and A. Chakrabarti, *J. Phys. Chem. A* **2008**, *112, 12303.*
56. J. Wang, M. Yang, G. Wang and J. Zhao, *Chem. Phys. Lett.* **2003**, *367, 448* .
57. K. Jackson, L. Ma, M. Yang, J. Jellinek, *J. Chem. Phys.* **2008**, *129, 144309.*
58. L. Pauling, *J. Am. Chem. Soc.* **1933**, *55, 1895.*
59. N. Bartlett, Proc. *Chem. Soc.* **1962, 218.**
60. M. Pettersson, L. Khriachtchev, J. Lundell and M. Räsänen, in *Inorganic Chemistry in Focus II*, edited by G. Meyer, D. Naumann and L. Wesemann (Wiley, Weinheim, **2005**), pp 15-34. See also, R. B. Gerber, Annu. Rev. Phys. Chem. **2004,** *55, 55 ().*
61. L. Khriachtchev, M. Pettersson, N. Runeberg, J. Lundell, M. Räsänen, *Nature* **2000**, *406*, 874.
62. S. Seidel and K. Seppelt, Science **2000**, *290*, 117.
63. P. Pyykkö and J. P. Desclaux, Acc. Chem. Res. **1979**, *12*, 276.
64. P. Pyykkö, Chem. Rev. **1988**, *88*, 563.
65. T. K. Ghanty, J. Chem. Phys. **2005**, *123, 074323.*
66. B. Kiran, X. Li, H.-J. Zhai, L.-F. Cui, and L.-S. Wang,, *Angew. Chem., Int. Ed.* **2004**, *43*, 2125.
67. T. K. Ghanty, J. Chem. Phys. (Communication) **2005**, *123*, 241101.
68. T. K. Ghanty, J. Chem. Phys. **2006**, *124*, 124304.
69. J. M. Thomas, N. R. Walker, S. A. Cooke, and M. C. L. Gerry J. Am. Chem. Soc., **2004**, *126*, 1235.
70. S. A. Cooke and M. C. L. Gerry, J. Am. Chem. Soc., **2004**, *126, 17000.*
71. P. Pyykkö, S. Riedel and M. Patzschke, *Chem. Eur. J.* **2005**, *11*, 3511.
72. T. Jayasekharan and T. K. Ghanty, J. Chem. Phys. **2006**, *124* 164309.
73. T. Jayasekharan and T. K. Ghanty, J. Chem. Phys. **2006**, *125*, 234106.
74. T. Jayasekharan and T. K. Ghanty, J. Chem. Phys. **2007**, *127*, 114314.
75. T. Jayasekharan and T. K. Ghanty, J. Chem. Phys. **2008**, *128*, 144314.
76. T. Jayasekharan and T. K. Ghanty, J. Chem. Phys. **2008**, *129,184302.*

After obtaining his M.Sc. degree in Physical Chemistry form Burdwan University, **Dr. Tapan K Ghanty** *joined BARC in 1988 through 32nd batch Training School and received Homi Bhabha Award for securing first rank among the Chemistry Trainees. He obtained his Ph.D. degree in Chemistry from Bombay University in 1996 for his work on density functional theory of chemical binding and chemical reactivity of molecular systems. He has spent two years (1997-99) at Chemistry Department, Indiana University, USA as a postdoctoral fellow. Dr. Ghanty is associated with various research areas starting from the development and generalizations of fundamental chemical concepts like electronegativity, hardness, polarizability, to large-scale first principle computations leading to the predictions of novel molecular and cluster species. His research interests include theoretical prediction of novel rare-gas compounds, computational investigation of structure and properties of hydrogen-bonded systems, supramolecular chemistry, electronic excited states, clusters and cluster assembled materials. He is also involved in the study of structure and bonding in lanthanide and actinide complexes relevant to nuclear waste management. Dr. Ghanty has co-authored 78 papers in peer reviewed international journals. He is the recipient of the DAE Scientific & Technical Excellence Award for the year 2008.*

Computational Chemistry to Process Systems Engineering

Sisir K. Sarkar
Radiation & Photochemistry Division, Bhabha Atomic Research Centre, Mumbai
sarkarsk@barc.gov.in

1. Introduction

Innovation is the process by which an invention, idea, or concept is converted into a real process, commercial product, or the like. Considerable pressure exists in the commercial sector to shorten the time frame and increase the yield of innovation from basic research, but there is no obvious pathway. Innovation in the chemical sciences -particularly starting at the level of basic research -is complex, often involving multiple interfaces with many more areas of science and technology. In today's environment multidisciplinary teams need to work in concert such that the real-time exchange of ideas, issues, and solutions results in concurrent development of multifaceted technologies.

Chemists want to understand not only the substances and transformations that occur in the natural world, but also those others that are permitted by natural laws. Consequently, the field involves both *Discovery and Creation*. Chemists want to discover the components of the chemical universe—from atoms and molecules to organized chemical systems such as materials, devices, living cells, and whole organisms. New chemical compounds are being created at the rate of more than *one million each year*. However, the number of possible molecules that are reasonably small and simple, exceeds the number of known compounds by a *factor well over* 10^{30}. Clearly, there is much to do and understand in the creation of molecules that do not yet exist. As part of the overall goal, chemical scientists also want to understand the biological properties of both natural and man-made substances - from molecular assemblies to cells to organisms.

Chemical Engineering emerged from applied chemistry by introducing an organized approach to the design of chemical process systems for manufacturing chemical products. The paradigm of *unit operations*— the individual steps of an overall process—characterized chemical engineering in the first half of the 20th century. During this time, the chemical industry, especially in the USA and Germany, was being built into a leading, and thriving, productive economic force. In the 1950s, and until the 1980s, chemical engineering research improved, advanced, and made more efficient both the design process and the ultimate designs of chemical plants. Academic research produced major advances in mathematical modeling and analysis—based on rapidly emerging new information on chemical kinetics, reaction mechanisms, and transport phenomena. This progress changed the process-design endeavor—from one based predominantly on empirical experience embodied in heuristics and correlations, to a more reliable, quantitatively predictive activity. By 1990s fundamental chemical research began to overlap with and penetrate chemical engineering to an unprecedented extent in the areas of polymers, catalysis, electronic materials synthesis & processing, bio-science and engineering, pharmacology & drug delivery, nano-science & engineering, and computational science & engineering.

In the present article, we would attempt to understand the way the field of chemical sciences - from fundamental, molecular-level chemistry to large-scale chemical processing technology has evolved, and the strong couplings / synergy that has developed between research in chemistry and chemical engineering.

2. Challenges ahead

In chemistry, standard subdivisions are analytical, biochemical, inorganic, organic, physical, and theoretical, while in chemical engineering they are: applied chemistry, kinetics, thermodynamics, transport processes, reaction engineering, process systems engineering,

and separations. These subfield categories are primarily used for pedagogical clarity and organizational management in academia, but they are not typically used in industrial chemical research and development.

There is no doubt that chemistry and chemical engineering have reached a high level of integration across the entire spectrum of the chemical sciences. Chemists - who have traditionally worked at the end of the spectrum nearest to pure, basic research - are also aware of the societal and technological benefit of their work. Indeed, such benefits are commonly referred to *justify the costs of the research.* Furthermore, chemists are increasingly involved in constructing, analyzing, and using complex systems and assemblies, from energy production to earth systems to cells.. The interplay between basic and applied research is *dynamic and cyclical*, [1] with mutual feedback spurring greater discovery and innovation. Some of the Challenges for Chemists and Chemical Engineers are identified as [2] :

- Develop *computer methods* that will accurately *predict* the properties of unknown compounds.
- Develop reliable computer methods to calculate the detailed *pathways* by which reactions occur in *both ground states and excited states*, taking full account of molecular dynamics as well as quantum and statistical mechanics.
- Invent *computer methods* to predict the *three-dimensional folded structure of a protein* and the pathway by which folding occurs-from its amino acid sequence, so information from the human genome can be translated into the encoded protein structures.
- Devise *experimental tests* to establish the *reliability* of new theoretical treatments.
- Develop new and powerful *computational methods*, applicable from the *atomic and molecular level* to the chemical process and enterprise level, that will enable *multiscale optimization*.

The increased computing power has profoundly influenced the Chemistry and chemical engineering like many other disciplines. All these has happened due to the phenomenal increase in speed and computational power of computers - as well as their dramatic reduction in cost - over the last decade. In terms of CPU speed, *Moore's law* implies that computing power should double every year or two, a pattern that is expected to continue for at least 10 years into the future. At the same time, key advances have been made in areas such as *ultraviolet lithography techniques*, non-leaking complementary metal oxide semiconductor *(CMOS)* transistors, and multiple instruction, multiple data *(MIMD)* computer architecture. In addition, the technology and software infrastructure now exist for researchers to routinely build large parallel supercomputing clusters using off-the-shelf commodity computers and networking components, thus increasing the impact of Moore's law by orders of magnitude. Over the years, it has been shown that the number of atoms in classical MD simulations has *doubled every 18 months in the past 36 years*, while that in quantum mechanical MD simulations has *doubled every 13 months in the past 15 years*. Finally, This has happened in part by enhancing many existing computational procedures, providing (i) new impetus to quantum mechanical and molecular simulations at the atomic level, and (ii) by optimizing processes and supply chain management at the macro system level.

3. Current Progress

Important insights have been obtained using approximate methods, not highly precise and excellent high-level methods for solving the Schrödinger equation have been developed. A Nobel Prize in 1998 went to John Pople and Walter Kohn for their different successful approaches to this problem. Earlier methods used many different parameters derived from experiment, but current so-called ab-initio methods as pioneered by Pople are essentially free of such experimentally derived parameters. With the current methods, systems of 5 to 20 common atoms are handled well. Density-functional theory (DFT) as developed by Kohn is also moderately successful with larger systems, and with more unusual atoms. In molecular

mechanics, force fields and sampling methods used in the calculations are being improved continually, but they are not yet good enough for atomic-level refinement of protein structures on a routine basis.

Initially, most theoretical methods calculated the properties of molecules in the gas phase as isolated species, but chemical reactions are most often carried out in solution. Biochemical reactions normally take place in water. In the simplest approach, solvents are treated as a continuum, whose average properties are included in the calculation. Explicit inclusion of solvent molecules in the calculation greatly expands the size of the problem, but newer approaches do this for at least those solvent molecules next to the dissolved species of interest. Reactions at catalytic surfaces present an additional challenge of handling the reactants and the atoms in the surface, as well as possible solvent species. The first concrete examples of computationally based rational catalyst design have begun to appear in publications.

In the area of collective properties, simulation methods have been developed to predict the phase equilibria of systems directly from force fields. Phase equilibria of various kinds (vapor-liquid, liquid-liquid, fluid-solid) lie at the center of most of the separation techniques (e.g., distillation and crystallization) in the chemical industry. The last decade has also seen dramatic improvements in molecular simulation methodologies - largely based on stochastic methods—for overcoming the long relaxation times inherent in the equilibration of polymers and similar complex materials.

A recent international comparative study of the industrial application of molecular modeling in the chemical, pharmaceutical, and materials industries in the United States, Europe, and Japan has been made and it showed remarkably diverse ways in which molecular modeling methods are successfully impacting industry today [3].

3.1 Chemical Supply Chain

Computational chemistry and Process systems engineering play a major role in providing new understanding and development of computational procedures for the simulation, design, and operation of systems ranging from atoms and molecules to industrial-scale processes. The enormous span of scales of space and time that range from computational chemistry to process systems engineering can be visualized with the "Chemical Supply Chain" [4] (Fig 1) :

The following points emerge from the chain :

- The supply chain starts with the set of chemicals that industry must synthesize and characterize at the molecular level.
- Next it aggregate these molecules into clusters, particles, and films - as single and multiphase systems that finally take the form of macroscopic mixtures.
- At the process engineering scale, the chain illustrates the design and analysis of production units that are integrated into a

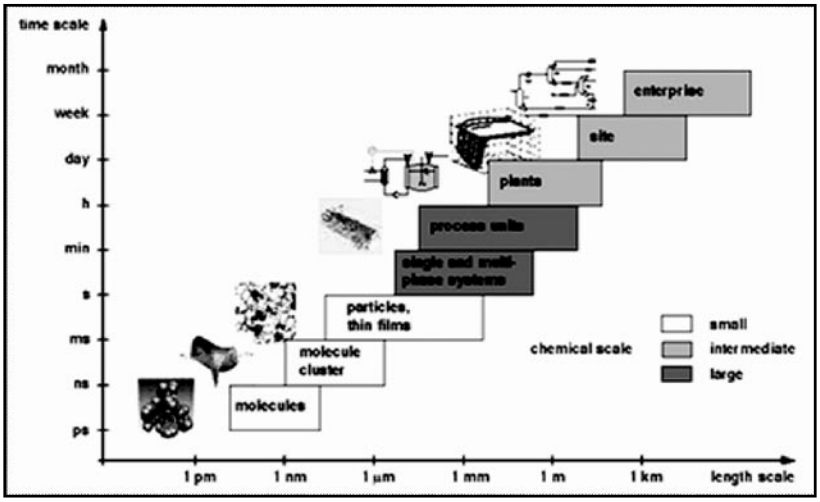

Figure 1 : *Chemical Supply Chain*

chemical process, which in turn is part of a site with multiple processes.

- Finally, this site is part of the commercial enterprise that is driven by business considerations.

The multiple scales of this chain are a fact of life in chemical sciences and technology. To date, the field has neither sufficient tools nor enough trained people to pursue computational chemistry and chemical engineering across all these scales. Advances in computing have facilitated major progress in computational chemistry and biochemistry, computational materials design, computational fluid dynamics, process synthesis, planning and scheduling, model-based process control, fault diagnosis, and real-time process optimization. This progress has been enabled by parallel advances in fundamental chemical physics theory, mathematics, operations research, and computer science - including computational techniques for simulation and optimization of chemical systems. Now let us look at how we can bridge length and time scales.

3.2 Bridging Length and Time Scales

Many of the problems cited already highlight the need for being able to bridge calculations across several length and time scales. For example, reactions involve changes in the molecules, and hence are inherently quantum mechanical in nature. But a reaction taking place in a solution at finite temperature implies that the reaction is influenced by a dynamic environment more pragmatically described by classical molecular simulation methods. Hence, a scale-bridging method is needed to allow the dynamics of the solvent around the reactants to influence the electronic structure of the reactants in various conformations, as well as the reactants influencing the motion of the solvent molecules around them.

One solution is to perform molecular simulations with force fields calculated "on the fly" by quantum mechanical methods at each time step. Such "first principles" or ab-initio molecular simulation methods are presently limited to fairly small numbers of atoms (around 100 to 1000) for rather short simulations (typically 10 ps). Other hybrid methods, which treat just the environment around reactants quantum mechanically, are less accurate in principle but allow much longer time scales and much larger spatial scales to be accessed, since the vast majority of the molecules are treated by classical molecular simulation.

The problem of spanning scales goes well beyond spanning from the electronic structure scale to the molecular (which might be thought of as the Ångström or nanoscale). Chemical processes at the commercial scale ultimately involve spatial scales on the order of meters, and time scales (corresponding to processing times in reactors and separations equipment) ranging from seconds to hours and, in the case of many bioengineering processes involving fermentations, days or weeks. In some cases, the connection is trivial: for low-molecular-weight molecular systems, properties calculated (a) at the electronic structure level (e.g., reaction rates, and free energies of formation and reaction) or (b) at the molecular simulation level (e.g., the so-called critical constants, and transport properties such as viscosity)can be used directly at the process scale as input data.

However, for complex molecules (such as polymers and proteins) the properties at the molecular level are not decoupled from the process level. For example, flow at process level can result in changes in the conformation of the molecules, which in turn changes the properties of the molecules. In such cases, the problem of developing accurate molecular modeling methods that will span the scales from electronic to molecular to mesoscopic to macroscopic cannot be avoided. Since such complex molecules and their processing are the focus of the modern chemical, pharmaceutical, and materials industries, it is imperative that the problem of developing effective *multiscale modeling* methods be solved. It is currently one of the most active research interest of the molecular modeling community. It is also a major focus of nanotechnology modeling efforts, since in such systems the need to connect nanoscale structure to macroscale functionality is even

more desirable.

Making the "scale-up" connection between the electronic and molecular structure of molecules and their macroscopic properties, and the design of processes to manufacture them, is one half of the story. The other half is making the connection "scale-down" from specification of a process-level manufacturing need (e.g., a solvent with better properties) to the design of a molecule that meets the need. Harnessing these yet-to-be-developed methods and combining them with state-of-the-art process modeling and optimization tools will result in integrated process and product design: the ability to computationally design and optimize products (e.g., chemicals, drugs, materials) as well as the manufacturing processes to make them.

The molecular modeling and process design communities recognize that, with the continued rapid pace of computer hardware, software, and algorithmic advances, this goal is now accessible in the next decade or two. Cross-fertilization between the fields has led to computational chemistry methods (e.g., simulated annealing) crossing over to the process design community, just as techniques from the process design community (e.g., mathematical programming methods) have crossed over to the protein folding community.

3.3 Tackling the Time Scales

The time scale problem was captured well by Chan & Dill in 1993 [5]. While parallel supercomputing makes it possible to span larger spatial scales rather easily, spanning larger time scales remains a fundamental difficulty. Even with fully efficient implementation on the world's fastest parallel supercomputers, Brute-force classical molecular dynamics simulation will not span the time scales present in complex molecular systems. The first ever microsecond-long molecular dynamics simulation of protein folding was reported which required *750,000 node hours* (equal to the product of the number of hours times the number of processors) of computer time on a Cray T3 supercomputer. According to Dill's prediction, this length of simulation was *not to be expected until around 2010*. However, as noted above, Dill's analysis does not take into account large-scale parallelization - which, unless the computation is communications limited, will effectively increase the speed of a computation in proportion to the number of processors available.

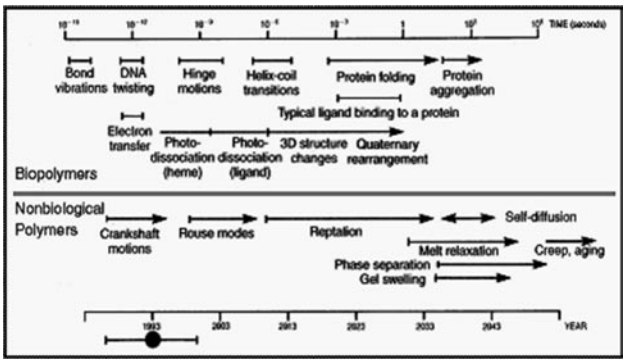

***Figure 2** : Time scales for various motions within bio- (upper) and nonbio-polymers (lower).*

To be more concrete, there are about 30 million sec in a year, and maximum speed at which messages can be passed between any two processors on a parallel supercomputer is roughly 10,000 per second. Hence, even if the time to compute forces could be reduced by sufficient parallelization to essentially zero, a molecular dynamics simulation could not execute more than 3×10^{11} time steps per year; When a calculation is limited by the time required to pass messages, it is referred to as communications-limited. Thus, with a time step of 10^{-15} s, in a year of computing the most one could hope to achieve is around 10^{-4} s of real time. This conclusion highlights the need to develop theoretically sound methods for spanning the many time scales present in the molecular simulation of complex systems (such as proteins and polymers).

The figure 2 shows the time scales for various motions within biopolymers (upper) and nonbiological polymers (lower). The year scale at the bottom shows estimates of when each such process might be accessible to brute force molecular simulation on supercomputers, assuming that parallel processing capability on supercomputers increases by about a factor of 1,000 every 10 years (i.e., one order of magnitude faster than Moore's law) and *neglecting new approaches or breakthroughs*.

4. The Tool Box

The chemical sciences are built on a set of fundamental mathematical theories that have increasing utility as computational hardware and software become more powerful.

4.1 Quantum Mechanics

As the basis for calculating the electronic structure of molecules, quantum mechanics permits calculations, often based on rational approximations, (i) of structure and properties of molecules, and (ii) of reactivity and reaction mechanisms. The Schrödinger wave equation can in principle predict the electronic states of any chemical species, but in practice it can be applied only approximately to molecules of any significant size. A continuing, important goal is to devise better and more accurate ways to obtain predictions of molecular structures, bond energies, molecular properties, transition state structures, and energies for systems of increasing size.

Good approximate quantum calculations usually can be done reliably only for isolated molecules. Another important objective in this field is to develop methodologies for *solvated molecules* and molecules that are *parts of membranes* or other *organized biological systems*.

Engineers are attempting to use quantum mechanical calculations to predict practical phenomena like (i) Making and breaking of bonds in adhesion and fracture - that are based on electronic interactions, (ii) Additional goals are to learn how to accurately include heavier elements and to calculate the properties of molecules as a function of time, when they are interacting with other species and (iii) Quantum calculations are the starting point for another objective of theoretical and computational chemical science: *multiscale calculations*. The overall objective is to understand and predict large-scale phenomena, such as deformation in solids or transport in porous media, beginning with fundamental calculation of electronic structure and interactions.

An important goal is to improve or supplement quantum mechanical methods in order to calculate reliably the energy and geometry of a transition state. This is one piece of information that can lead to the larger objective of predicting

(a) Rates of unmeasured reactions : reaction rates also depends on our knowledge of dynamical properties of molecules and the *dynamics of their sampling* of accessible electronic, rotational, and vibrational states.

(b) Course of excited state reactions i.e., photochemical transformation : the development of successful theoretical treatments for such complex phenomena presents a substantial challenge.

(c) Catalytic activity of a given surface for a particular reaction : using computational quantum chemistry, it is becoming possible to predict with reasonable accuracy the energy barriers and transition states of molecules reacting on catalytic surfaces, thus leading to insights into reaction rates. This is enabling a new field of rational catalyst design.

4.2 Molecular Mechanics

Another tool for working toward this objective is *molecular mechanics*. In this approach, the bonds in a molecule are treated as classical objects, with continuous interaction potentials (sometimes called force fields) that can be developed empirically or calculated by quantum theory. This is a powerful method that allows the application of *predictive theory* to much larger systems if sufficiently accurate and robust force fields can be developed.

Predicting the structures of proteins and polymers is an important objective. The ability to model isolated polymer molecules (in dilute solution) is well developed, but fundamental molecular mechanics models of dense systems of entangled polymers remains an important goal.

Similarly to predict protein structure from the amino acid sequence - to calculate how polypeptides fold into the compact geometries of proteins. and how a proposed drug might bind into a protein can also be explored by molecular mechanics model.

4.3 Modeling and Simulation

Modeling and simulation are extremely important tools in the chemical sciences. The

understanding and engineering of complex chemical processes, such as combustion or atmospheric chemistry and transport generally rely heavily and increasingly on modeling and computation. Modern computer methods - including molecular graphics, simulations, and animations - have greatly enhanced the ability of scientists and engineers to understand and utilize the results of their computations.

Yet modeling can be no better than its assumptions. It often suffers from the problem that we cannot follow any computed process for a long duration (many time steps) primarily because the computer time needed per time step is significant, but also because of the cumulative propagation of round-off errors.

The typical time step is ~ 1 femto second of real time for an atomically detailed molecular simulation. Consequently, modeling phenomena on the femto second time scale would require about 10^3 time steps, which is not difficult, and modeling on the picosecond time scale (10^6 time steps) is fairly routine. However, many phenomena of interest (e.g., the time to fold a protein) are on the millisecond or longer time scale and would require 10^{15} time steps or more. One approach is to use stochastic methods based on cleverly chosen Monte Carlo methods; another is to reduce the level of detail in the models for the molecules (so-called coarse grained models).

4.4 Statistical Mechanics and Fluid Mechanics

Statistical mechanics is the science that deals with average properties of the molecules, atoms, or elementary particles in random motion in a system of many such particles and relates these properties to the thermodynamic and other macroscopic properties of the system. Sometimes the theoretical or computational approach to description of molecular structure, properties, and reactivity cannot be based on deterministic equations that can be solved by analytical or computational methods.

Molecules and assemblies of molecules exist in distributions of configuration, composition, momentum, and energy. Sometimes, this statistical character is best captured and studied by computer experiments: molecular dynamics, Brownian dynamics, Stokesian dynamics, and Monte Carlo methods. Interaction potentials based on quantum mechanics, classical particle mechanics, continuum mechanics, or empiricism are specified and the evolution of the system is then followed in time by simulation of motions resulting from these direct inter particle, stochastic, or fluid mechanical forces.

Simulations and statistical mechanics are key tools for physical chemists and engineers working on understanding rheological behavior, mass transport, modeling of microfluidic devices, flow of granular media, and behavior of dense particle suspensions. At the next higher level of coarse-graining, *fluid mechanics* and other continuum mechanics methods are active arenas of theory and computation. For example, electro-rheology and magneto-rheology have provided tremendous impetus in the last decade.

The links between the thinking of chemical engineers studying transport and chemists designing and producing materials are crucial for progress. *Granular media* is another area where the clear interplay between science and technology is facilitating progress. From the viewpoint of computation and simulation, engineers working in granular media are addressing problems of flow and mixing (such as those arising in the processing of powdered pharmaceuticals) with discrete computational approaches encompassing particle dynamics, Monte Carlo, and cellular automata calculations.

Now we will demonstrate the linkages described so far by taking two case studies [6] (*Courtesy : Venkat Venkatasubramanian, Prof. Chemical Engineering at Purdue University*) and finally conclude by looking at the acceptance of computational chemistry tools in a variety of industries,

5. Case Studies

(1) The first example is a case study in the *molecular design of fuel additives*. U.S. Environmental Protection Agency (EPA) has mandated a test in a standardized engine before a fuel can be sold. The BMW engine is run for 10,000 miles; then it is taken apart. Deposits on the valve are measured to determine the intake valve deposit (IVD). The

IVD needed < 100 mg before the fuel could be sold. There is a whole market for fuel additives, which trap undesirable molecular fragments and prevent them from depositing on the surface of the valve. The problem is how to design these fuel additives to minimize the IVD and ensure it is 100 mg or less. To exhaustively test all possibilities is very expensive, because for every 10,000-mile test the engine must be disassembled to measure the IVD. Every single data point costs about $10,000 and a considerable amount of time. Therefore, it was required to develop a model-based approach to this problem.

In the traditional design method after the molecule or formulation is made, it is evaluated to see whether it meets the objectives. If the process is not successful, it begins again. This typical guess-and-test methodology yields a very long and expensive cycle. Clearly there is a need for a more rational approach, which will remove some of the guess-and-test elements. These problems are so complex that guessing and testing cannot be completely eliminated, but the development of a system that can increase efficiency can help.

Computer-aided design, in this case of fuel additives, makes the design cycle much shorter and more efficient by more narrowly directing the molecular search. Expecting the EPA to lower the IVD value further in the future, Lubrizol asked to design a fuel additive for an IVD of 10 mg. A genetic algorithm in the hybrid model was used to predict the properties of some designed molecules. One structure which came close to the target (12 mg IVD with 99.3% fitness) has been already discovered by the Lubrizol scientists through their intuitive guess-and-test approach. However, the hybrid model discovered two other better structures. The best of the three had completely novel chemistry and was a combination of molecules that had never been thought of. The hybrid model used *"out of the box thinking"* that opened up possibilities of new chemistry for generating leads in a much shorter time frame

(2) A second problem involves Caterpillar, which sells *earth-moving equipment*. This equipment is largely made of metal – 99% iron - however, there are more than 1,000 rubber components in these machines, including tyres, hoses, gaskets, and other parts. This equipment is used in *oil wells in Siberia in the winter* as well as *oil fields in Kuwait in the summer*. This multimillion-dollar machine becomes idle because a $1,000 rubber component failure because of the extreme operating conditions. This is a major product liability, and warranty headache for Caterpillar.

Component failure is so crucial that Caterpillar does not trust any other company to make these rubber products—not even Goodyear or Firestone. Caterpillar makes its own rubber component formulations. Rubber component failure is a multilevel issue:

- performance depends on the rubber parts, which depend on
- the rubber component-based materials which in turn depends on
- the failure mechanics properties of these materials affected by
- the rubber curing chemistry.

An the end, the design and manufacturing related issues depend on *quantum chemistry of sulfur links*. This is another problem in which the transformation process goes from *molecules to materials to market.* Many things go into rubber, including *activators, sulfurs, retarders, accelerators, and so on*. A very interesting and complex set of approximately *820 reactions occur that result in curing*. Current models cannot handle so much information; we need a more complex modeling environment for this type of situation. Of the top 3 formulations the model designed, one meets the design criteria, but degrades much more quickly than desired. The other two formulations have much better degradation kinetics. Given the situation in which some high-level chemistry is hypothesized, too much data exist for one scientist to analyze. We require *modeling infrastructure* to handle such data explosion.

6. Summary

From modest beginnings, many companies have now developed effective molecular modeling activities. A few example of companies and their activities including the development of products and processes are as follows:

- Bio-active materials like pharmaceuticals (Merck, Novartis, Takeda Chemicals) and crop-protection chemicals *(DuPont, Sumitomo Chemical)*
- Polymers, glass, and structural materials *(Asahi Chemicals, Owens Corning, Rhône*)
- Electronic and photonic materials *(Motorola, Toshiba, Lucent)*
- Homogeneous and heterogeneous catalysts *(Ford, Haldor Topsøe, Ube Industries)*
- Sorbents for gas separations *(BG Technologies / Advantica Technologies Ltd., Air Liquide, Air Products and Chemicals)*
- Personal-care, food, and consumer products (*Colgate Palmolive, Unilever, Kellogg, 3M)*
- High-volume chemicals and materials *(Dow, BASF, Rohm & Haas)*
- Dyes and pigments *(Bayer, Mitsubishi)*
- Films and imaging *(Fuji Photo Film, Xerox)*
- Fuels and automotive chemicals (*Chevron, TotalFina / TotalFinaElf, Lubrizol)*
- Commercial software and hardware for calculations *(MSI / Accelrys / Pharmacopeia, Gaussian, COSMOlogic, Fujitsu)*

In the final analysis, basic understanding of chemistry will require *new approaches or breakthroughs*. Presently there is no hope that we can directly observe a chemical reaction in its full molecular detail on the fast and microscopic scale on which it occurs. As discussed above, simulation and modeling are central components of process engineering. Improvements in these techniques will lead to the design of much more efficient processes. Integrating the current and future capabilities of computational chemistry and process engineering will result in improved chemicals, materials and pharmaceuticals; yield more efficient green processes to manufacture them; and accomplish this while providing greater financial return.

10. References & suggestive readings

1. Pasteur's Quadrant, Donald E. Stokes, Brookings Institution Press, Washington, D.C., 1997
2. C& EN, 78 (14) p.5 April3, 2000; Beyond the Molecular Frontier: Challenges for Chemistry and Chemical Engineering, National Research Council, 2003
3. WTEC Panel Report on Applications of Molecular and Material Modeling, Kluwer Academic Publishers, 2002
4. Chemical Supply Chain; Courtesy Prof Wolfgang Marquardt, Instt of Process System Engg, RTWH, Aachen, Germany
5. H.S. Chan and K. A. Dill. *Physics Today, 46, 2, 24, (1993)*
6. Reducing the Time from Basic Research to Innovation in the Chemical Sciences: A Workshop Report to the Chemical Sciences Roundtable, National Research Council, 2003

- Chemistry Today and Tomorrow: The Central, Useful, and Creative Science, Ronald Breslow, American Chemical Society, Washington, D.C., 1997
- Technology Vision 2020: The U.S. Chemical Industry, The American Chemical Society, American Institute of Chemical Engineers, Washington, D.C., 1996
- The Future of U.S. Chemistry Research: Benchmarks and Challenges Committee on Benchmarking the Research Competitiveness of the United States in Chemistry, National Research Council, 2007
- Rising Above The Gathering Storm: Energizing and Employing America for a Brighter Economic Future: National Academy of Sciences, National Academy of Engineering, Institute of Medicine, 2007

Dr. Sisir K. Sarkar *is presently the Head, Radiation & Photochemistry Division, BARC. He is also the Vice President of ISRAPS. His research interest includes radiation & photochemistry with lasers and accelerators, chemical dynamics, spectroscopy and laser development.*

Hydrophobic Hydration at the Nanoscale

Niharendu Choudhury
Theoretical Chemistry Section, Chemistry group, Bhabha Atomic Research Centre, Mumbai 400 085, India
email: nihcho@barc.gov.in

Abstract

It is well known that hydrophobic effect plays a crucial role in the hydration and self assembly processes over the entire length scales ranging from solubility of inert gases in water to folding of proteins and other macromolecules in aqueous solution. However, precise role of water in the process remains unclear till date. Water in general is mysterious and interfacial water in the vicinity of an extended hydrophobic surface is even more mystifying due to the complex interplay of its long-ranged interactions with bulk water and short range interaction with the atoms of the hydrophobic solute surface. Existence of a dewetting transition near an extended hydrophobic surface is believed to be responsible for the self assembly of hydrophobic nanoscopic objects in the aqueous environment. In this article, we discuss the subtleties in the behavior of water in the interfacial region with respect to minute details of the generally weak and neglected dispersion interaction and the topology of the solute.

Introduction

Hydrophobic effect[1-3] has been well recognized over the years as the dominant driving force[3] in a wide range of physiochemical and biophysical phenomena as diverse as protein folding, the formation of membranes, micelles, various complex mesophases in the surfactant solutions, formation of amyloid plaques in the brain tissue causing neurodegenerative diseases and self assembly of various hydrophobic nanomaterials. Oil and water do not mix because they dislike each other--was the primitive view of hydrophobic effect. In early days, association of hydrophobic solutes in water has been thought to be a result of the formation of chemical bonds, like all other covalent bonds. Most likely, with that view of covalent bonding, Walter Kauzmann in 1954 coined the term 'hydrophobic bonding'. However, eventually it became clear that noncovalent association is fundamental to aggregation or self organization relevant to biological and many chemical processes. Since that time, extensive efforts have been made to understand the hydrophobic effect and its actual role in the aggregation of macromolecules in water. Although several experimental and theoretical investigations have enriched our knowledge on hydrophobic effect, multifaceted nature of the same has resulted lots of debates and controversies. Formation of hydrogen bonding among hydrophilic backbones and in some cases formation of disulphide bonds are the driving forces in the initial stages of protein folding resulting in formation of extended surfaces such as beta sheets and strands in a protein. However, presence of agglomeration of hydrophobic groups deep inside the core of a protein in its native state as obtained by x-ray crystallography suggests the effective interaction between hydrophobic groups in water to be attractive in nature.

At the small length scale where one deals with the dissolution of atomic size inert gases and small alkanes in water, concept of hydrophobicity is well recognized. Hydrophobic effect as emerged from experimental and theoretical investigations on the solubilities of small inert gases and hydrocarbon molecules, has the trademark temperature signature of large, positive heat capacity changes on dissolution. On the other hand, many soluble proteins also have the puzzling temperature signature in the sense that these proteins unfold both upon heating and cooling. The fact that the solubilities of nonpolar gases are nonmonotonic, surfactants display a minimum in their critical micelle concentrations with respect to temperature and proteins undergo hot and cold denaturation leads to a common underlying mechanism in all these cases. Thus dissolution of small hydrophobic molecules in water and the protein folding are the two extreme

ends of the same spectrum, interlinked with each other through the concept of hydrophobicity.[3] Given the complexity of the protein topology and interactions, direct extrapolation of the small lengthscale results to explain association and assembly at larger length scales leads to the discrepancies and creates puzzlement.[4,5]

In fact, length scale dependence of the manifestation of hydrophobicity has been sought[6] to be the reason for the puzzlement in understanding the role of hydrophobicity. As the phenomena like protein folding, micelle formation and aggregation of hydrophobic nanoparticle in water involve a large number of small hydrophobic units extending over a large length scale, manifestation of hydrophobicity would be different from the same at smaller length scale relevant to solubility of inert gases. Potential of mean force (PMF) is the free energy change in bringing two solutes at a particular intersolute distance from the completely dissociated state (where the two solutes are far separated). The decomposition of the PMF into direct solute-solute interaction (in vacuum) and the contribution arising from solvent participation (which is commonly known as solvent induced PMF) helps us in estimating the effect of solvent. The solvent induced PMF between two hydrophobic solutes in water is thus a measure of the extent of effective interaction between the two hydrophobes in a solvent medium. In the small length scale relevant to dissolution of inert gases in water, the PMF has the usual signature of contact pair minimum (where two solutes are in contact) as well as a solvent separated minimum separated by a desolvation barrier (see Figure 1(a). The first minimum is for the contact pair state and the second minimum is for the solvated state with one intervening water layer between the two small hydrophobic solutes. The barrier between the two minima is known as desolvation barrier.). On the other hand, at the large length scale, using purely repulsive model of the hydrophobic solutes, it has been demonstrated[6–10] that the PMF (see Fig. 1(b)) between two large hydrophobic plates in liquid water is strikingly different from the same between two small solutes like methane in water. Below a critical distance the PMF of the

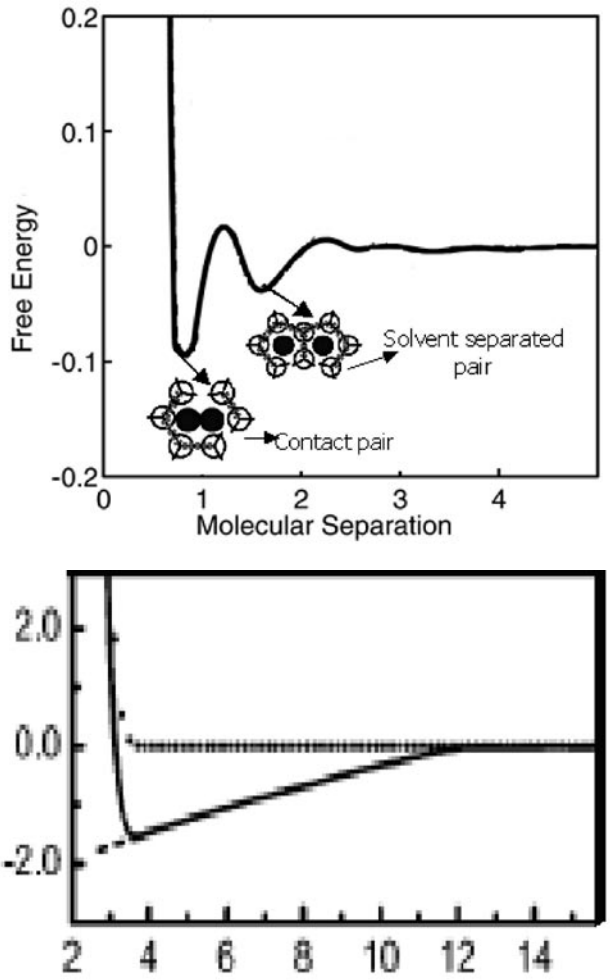

***Figure** 1: Potential of Mean Force (PMF) of two (a) methane molecules (b) two large hydrophobes in water.*

former is monotonically attractive and without the usual desolvation barrier and the first solvent separated state (compare Fig. 1(a) and (b). The second minimum of Fig. 1(a) corresponding to the first solvent separated state is absent in Fig. 1(b)). The attractive PMF is a consequence of the dewetted intersolute region, which causes dewetting induced collapse of the hydrophobic solutes.[9,10] Stillinger[11] was the first to envisage that in the vicinity of a large hydrophobic solute due to the breaking of hydrogen-bond network of water, a thin vapor layer around the extended hydrophobic surface is formed. When two such solutes come close to each other fluctuation in the liquid-vapor interface around the individual solute causes remaining water molecules to be expelled from the intersolute region. Based on a square gradient like functional, which is widely used to study liquid-vapor interface, Chandler

and coworkers[10] have developed a self-consistent theory for the calculation of the density of water near a hydrophobic solute and solvation free energy. Based on the results of the theory[10] and molecular dynamics simulation[7] using purely repulsive solutes, it has been demonstrated that dewetting mediated attraction between the two large hydrophobes is the reason for hydrophobic self assembly at the large length scale.

In all these studies, hydrophobic solute is modeled as hard sphere or purely repulsive soft sphere. However, in all real solutes there is considerable dispersion interaction, without which existence of liquid phase is not possible. The role of the small attraction arising from the solute-water van der Waals interaction on the behavior of water in the nanoscopic confinements has been further realized in the study of Hummer et al[12] on the water behavior in and around a small carbon nanotube (CNT). By considering explicit interaction between the water and the carbon atoms of the CNT, it has been demonstrated that water occupy the completely hydrophobic interior of the CNT in the form of single chain and the confined water are thermodynamically stable. Although there are only 2 hydrogen bonds per water molecule inside CNT as compared to around 4 in the bulk water, stability of the one dimensional chain of water inside the CNT has been explained in terms of binding energy distribution, which is shielded inside the CNT from fluctuations prevalent in the bulk.[12] Similarly, use of realistic van der Waals interaction instead of purely repulsive part of it, results in the decrease of the critical distance of dewetting between two nanoscopic hydrophobic solutes. This observation[8] clearly calls into question the role of dewetting transition in the protein folding process. The magnitude of attractive dispersion interaction even for a hydrophobic side chain like methyl group as obtained from state of the art quantum chemical calculations is not negligibly small. Given the fact that protein backbones are made up of heteroatoms with significant polarity and dispersion interaction, careful consideration of attractive van der Waals interaction is of important in understanding the mechanism of protein folding.

In fact, it has been demonstrated[9] recently that the mechanism of assembly is different in the cases of solutes with and without dispersion interactions. When no dispersion interaction is considered, stabilization of the contact pair state arises solely from solvent induced contribution, while for solutes with dispersion interaction, a considerable amount of stabilization arises from direct van der Waals interaction between the atoms of the two extended hydrophobic solutes.[9] Unlike purely repulsive case, intersolute dewetting has not been observed in the case of solutes with dispersion interactions. However, puzzlement arises from some recent investigations, in which the existence of intersolute dewetting has been observed even in the case of realistic models with considerable dispersion interaction. Koishi et al.[13] have found intersolute dewetting even though the individual attractive solute-water interaction is stronger than the same used by Choudhury et al.,[9,14] who found a completely wet intersolute state. The existence of drying in the interdomain region of a protein[15] on one hand, and the disappearance of dewetting in the case of another protein[16] also creates puzzlement in understanding the role of attractive dispersion interactions. All these results indicate that apart from the influence of attractive solute-water dispersion interaction, the topology of the solute might be playing a very important role in the hydration and dewetting at the nanoscale. In this article, we present our results demonstrating the effect of solute topology on the solvation structure of large hydrophobic solutes in water and the consequence of it on the dewetting transition. In particular, we have investigated the effect of solute topology on the structure as well as dynamics of water under hydrophobic confinement.

Models and methods

All the results presented here have been obtained from atomistic molecular dynamics (MD) simulation. We investigated behavior of water in and around two large, flat hydrophobic solutes. Water molecule was modeled with standard SPC/E model and each of the hydrophobic solute was modeled as paraffin-like plates, each of which

was constructed by arranging n-$C_{18}H_{38}$ molecules in parallel in such a way that all of the carbon atoms lie on the same plane. Two solute plates were placed symmetrically at a fixed intersolute distance r_0 around the center of a cubic box containing anything between 1800-2500 water molecules (depending on the solute size), with the plates being parallel to each other as well as to the xy-plane. The overlapping water molecules from the immediate vicinity of the two plates were removed followed by a steepest decent minimization. Potential parameters for the alkane molecule were taken from united atom OPLSUA[17] force field. The topology of the plate was varied by changing the intermolecular spacing, a_0 (see Fig.2(a)), between different C_{18} molecules in a plate. Three plates with a_0 values of 4, 5, and 6 Å were used. In some cases paraffin plate with a_0 = 7 Å was also used. The sizes of the above three plates as measured by the center-to-center distances between the end CH_3 or CH_2 groups were 16, 20, and 24 Å, corresponding to the edge-to-edge distances (using van der Waals radii) of approximately 20, 24, and 28 Å, respectively. For all the plates, potential parameters of the CH_3 and CH_2 groups remained the same. For the solute-water interaction, the cross parameters for the LJ potential were obtained from the Lorentz-Berthelot mixing rule. The simulations were performed in an isothermal-isobaric (NPT) ensemble with the molecular dynamics extended system approach of Nose and Anderson. Details of the simulation can be found elsewhere.[9,18]

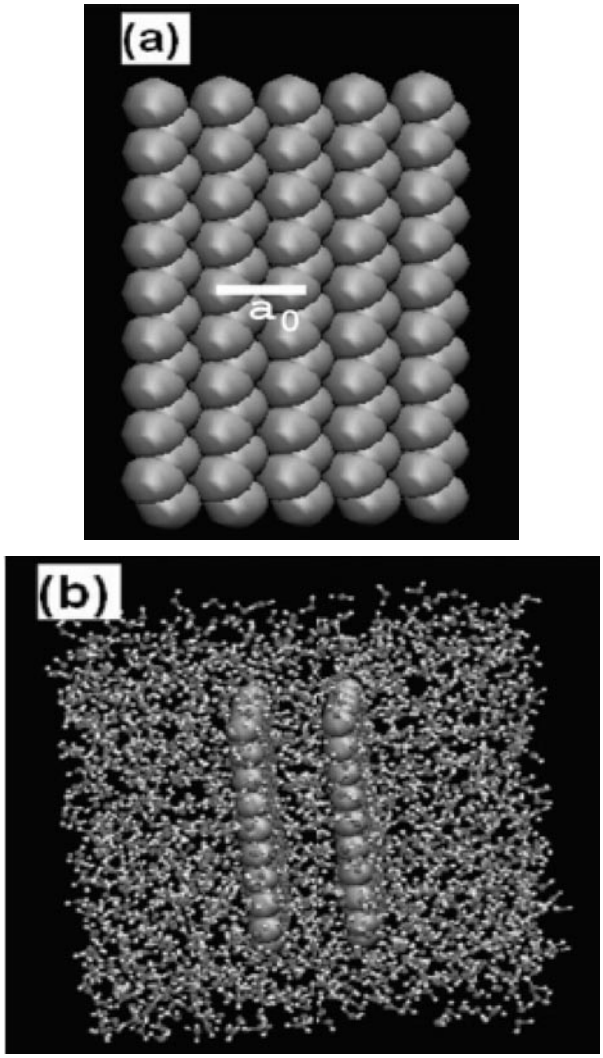

Figure 2: *(a) VDW representation of the paraffin like plate. Intermolecular distance a_0 of the plate is shown by a white line. (b) A snapshot of a simulation box with a pair of paraffin plates in water.*

Spatial structure of water in the intersolute region

In Fig. 2, a model paraffin like plate (left) and a two-solutes system immersed in water (right) as used in the present simulation study are shown. In order to get an idea about the water accessibility in the intersolute region, position dependent density of the water molecules has been calculated in and around the plates. We have presented here the structural and dynamical behavior of water in and around three different sets of model hydrophobic paraffin like plates differing from each other only in the intermolecular spacing (a_0) between two adjacent paraffin molecules within the plate.

The normalized ensemble averaged number density distribution, $\rho(z)/\rho_0$ (ρ_0 being the bulk density) of water in and around the two-solutes system with a_0 = 4, 5 and 6 Å at an intersolute separation r_0 = 7.2 Å corresponding to one-layer of intervening water molecules has been presented in Fig. 3. It is to note that for the topology and the forcefield used here, the intersolute region at r_0 = 7.2 Å is geometrically sufficient to accommodate single layer of water molecules. The density distributions of water molecules as obtained from the MD simulation reveal significant water accumulations (twice as that of bulk density) on the outside surfaces of the plates in all the three

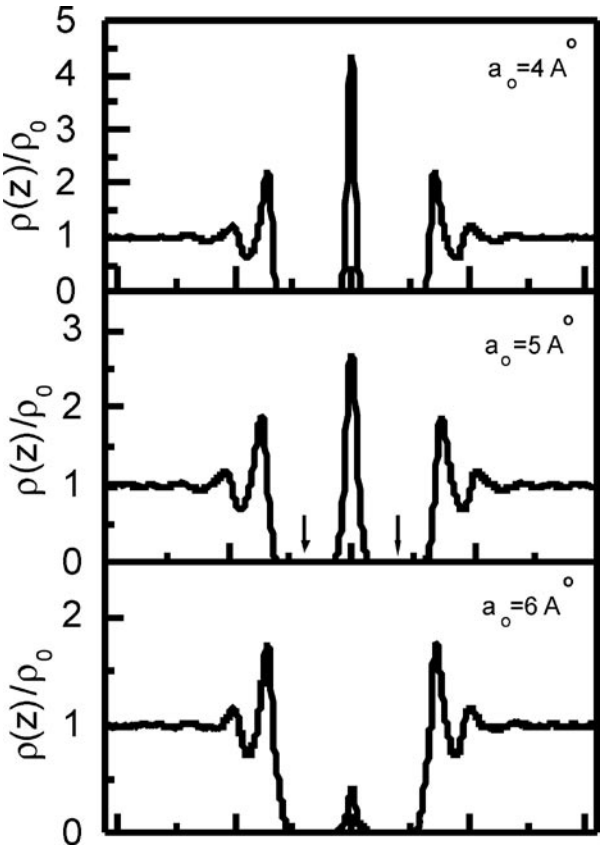

***Figure** 3: The normalized single particle density $\rho(z)/\rho_0$ of water oxygen in and around three different plates with intermolecular spacings (a) a_0 = 4 Å (b) 5 Å and (c) 6 Å.*

sets (with a_0 = 4, 5 and 6 Å) of plates. Striking difference in the peak heights for the three plate-water systems has however been observed in the middle of the two plates. For a_0 = 4 Å plates (see Fig 3(a)), there is a large sharp peak in the middle, indicating the water density in this region is more than four times the bulk density. However for the a_0 = 5 Å plates, in which paraffin molecules are slightly sparsely packed (i.e. solute atom density is slightly less than that in the former case), the density peak (see Fig. 3(b)) of water in the middle has been decreased to around 2.5, indicating partial dewetting in the intersolute region. Significant reduction in the density of water in the intersolute region has been observed in the case of a_0 = 6 Å plates. In this case, there are almost no water molecules in the middle as represented by a small, diminished density peak (see Fig. 3(c)) in the middle. Before concluding anything from this set of results, we should remember that the density profile shown in this figure is an

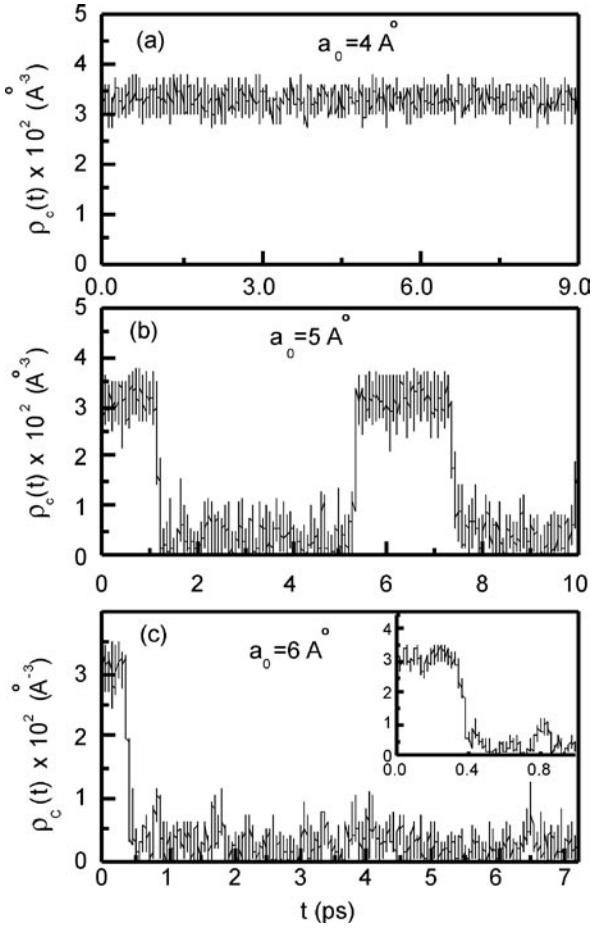

***Figure 4:** Plot of the instantaneous number density of water, $\rho_c(t)$ in the intersolute region corresponding to Fig. 3.*

ensemble averaged quantity, which does not give any information about fluctuations in the number density of the water molecules in the intersolute region. In order to monitor fluctuation in density in the intersolute region, therefore, instantaneous number density $\rho_c(t)$ of the water molecules is a better order parameter. The instantaneous number density $\rho_c(t)$ of the confined water for a_0 = 4 Å plates as shown in Fig.4(a) reveals that the intersolute region remains wet or filled through out the simulation time of 9 nanoseconds, without any large fluctuation leading to a dry or a partially dry state. It is consistent with the one-particle density distribution of Fig. 3(a). Thus, the solute-water system with a_0 = 4 Å as presented here shows persistent wetting in the intersolute region. Similar wet interface has been observed in many other recent investigations.[9,12,14,15,18,19] On the contrary, the instantaneous density $\rho_c(t)$ of confined water for a_0 = 6 Å plates (see Fig. 4(c))

is very high initially as the simulation has been started from the wet (completely filled) intersolute state. However, after 400 ps almost all the water molecules get expelled from the intersolute region leading to a dewetted state (as represented by a very small value of $\rho_c(t)$). After 400 ps, there is no large fluctuation leading to the wet state. Thus, the huge reduction in equilibrium density peak as shown in Fig. 3(c) is a result of persistent dewetting as observed in the instantaneous density plot presented in Fig. 4(c). The dewetted intersolute region has been observed in many earlier investigations.[7,8,10,11,13,16] In case of a_0 = 5 Å plates (see Fig. 4(b)) a very interesting feature of the instantaneous density of water in the confined region has been observed. The intersolute region was completely wet for a long time of more than 1 ns. Again, as the system entered into an almost dewetted state, it stayed there for a time as long as 4 ns and after that it enters the wet state again. As it is found here and also in many recent inve stigations,[12,14,18,20] the behavior of water confined between two large hydrophobic solutes is subtle with intermittent wet-dry transitions with a lifetime of a few nanoseconds. In the present case, within the 10 nanoseconds time scale explored, the system has visited each of the dry and wet states twice. It is important to note that the potential parameters of the individual atoms of the plate and the water are the same for all the model plates of this study. Thus, the differences in structural changes of water in the intersolute rsgion for the three different sets of plates are a consequence of the effect of topology of the plate. In the case of a_0 = 4 Å plates, because of the denser atomic arrangement of the solute atoms, a water molecule in the intersolute region experiences a stronger attractive van der Waals interactions of the solute atoms as compared to other two sets of solute plates. Therefore, water accumulates in the intersolute region leading to the wet state. In the case of a_0 = 6 Å plates, due to sparsely arranged solute atoms, solute-water attractive dispersion interaction is so feeble that water does not prefer to stay in the intersolute region. Instead they move away into the bulk, where extent of hydrogen bonding is more, and leading to a greater stability. In case of a_0 = 5 Å plates, the van der Waals interaction is intermediate between the two above mentioned cases and the free energy surface of the composite solute-water system contains two minima of almost equal well depth in its free energy surface corresponding to wet and dry intersolute states. Therefore, the system shuttles between the two as a function of time. Similar wet-dry oscillations have been observed in other investigations involving carbon nanotubes and biological ion channels.[12,18,20]

Dynamics of confined water

Dynamical properties of a fluid are generally obtained by calculating a normalized time correlation function c(t) of the form

$$c(t) = < \sum_{i=1}^{N} f_i(t+t_0)\ f_i(t_0) > / < \sum_{i=1}^{N} f_i(0)\ f_i(0) > \quad (1)$$

where $f_i(t)$ is a vector function of positions and/or velocities of a molecule i at time t. Angular brackets denote averaging over time origins t_0.

TABLE I: Ftting parameters P and α for $\Delta r_{||}^2$ (t) of water for the three different plate- water systems

a_0 (Å)	P	α
4.0	1.197	0.935
5.0	1.189	0.979
6.0	1.549	0.939

Our intention is to investigate the effect of intermolecular distance (a_0) within the paraffin plate (the hydrophobic solute) on the dynamics of water in the interplate region, particularly in a state from which onset of dewetting occurs (i.e one stable layer of water molecules between the two plates). For analyzing translational dynamics of confined water between two plates, we have calculated overall mean square displacement,

$$\Delta r(t)^2 = [x(t) - x(0)]^2 + [y(t) - y(0)]^2 + [z(t) - z(0)]^2 \quad (2)$$

as a function of time as well as velocity autocorrelation function of oxygen atoms of the water molecules in the intersolute region. The mean square displacement (MSD) plots of intersolute water molecules for all the three types of plates are shown in Figs 5. The manifestation of the effect of topology (intermolecular distance, a_0) of the plate is quite prominent. The slope of the MSD for water in the intersolute region of

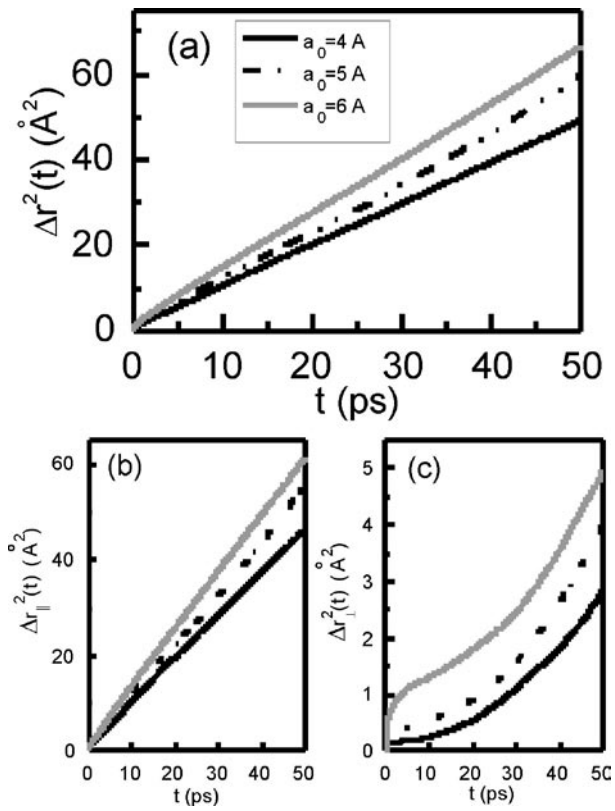

***Figure** 5: (a) The overall mean square displacements, <Δr²(t)> of water oxygen in the confined region with three different topologies of the solute plates. (b) The same as in (a) but for the projection of the MSD (<Δr$_{||}$²(t)>) parallel to the plates. (c) The same as in (b) but for the projection of MSD (<Δr$_{\perp}$²(t)>) perpendicular to the plate*

the plate with a_0 = 6 Å is greater than that for the plate with a_0 = 5 Å. The MSD for a_0 = 4 Å plate has the lowest slope among all the three (see Fig. 5). Thus, there is reduced translational mobility of water in the intersolute region for a_0 = 4 Å plates as compared to the same for the other two plates. The translational diffusion coefficient of the water molecules is related to the slope of the MSD by the Einstein relation,

$$D = \frac{1}{6} lim_{t\to\infty} \frac{<\Delta r^2>}{\Delta t} \qquad (3)$$

where Δt is the time difference corresponding to the measured MSD <Δr²(t)>. Extraction of D from the Einstein's relation is based on the linear relation of MSD with time t at long time (normal diffusion). In the present case, a linear fit to the MSD data does not yield a good fitting criterion (as the χ^2 value is high and around 0.3). Thus, the translational dynamics of water in the hydrophobic confinement is anomalous in the sense that the MSD of confined water is not perfectly linear in time. However, diffusion in the confined system is expected to be highly anisotropic and due to the specific symmetry of the planar interface studied here, the diffusion in the direction parallel to the plates are quite different from the same along the perpendicular direction. Since the system is confined in the z-direction (perpendicular to the plane of the plates), it may be argued that the anomalous diffusion may be a result of anisotropy in the z-direction, along which Einstein relation is not valid.[21] In order to resolve the issue, we have decomposed the MSD (<Δr²(t)>) into parallel and perpendicular directions of the plates. The MSD parallel to the plate, <Δr$_{||}$²(t)> (= < (x(t)−x(0))² +(y(t)−y(0))²) >) as shown in Fig. 5(b) also does not vary linearly with time (the χ^2 value of the linear fit is 0.38) indicating that the diffusion under hydrophobic nanoconfinement is inherently anomalous and it is not a consequence of the anisotropic z-component of the MSD.[26] In order to quantify the deviation from normal behavior, we have fitted <Δr$_{||}$²(t)> data with the equation: $< \Delta r_{\|}^2(t) >= Pt^{\alpha}$, where the exponent α is a measure of deviation from the normal behavior and the parameter P is a measure of mobility of the particle in the given environment. The value of α is 1 for a true Brownian diffusion observed in normal bulk liquid. In this case, we obtain a better fit with χ^2 around 0.02 or less in most of the cases. From the values of α in Table I it is evident that water diffusion in hydrophobic nanoconfinement is sublinear. It is important to notice that the MSD along the perpendicular direction, <Δr$_{\perp}$²(t)> is highly nonlinear and the displacements in this direction are very small (see Fig 5(c)). The sublinear behavior (α < 1) of MSD has been observed in many earlier studies of water in nanoscopic hydrophobic confinements,[22,23] hydration water of hydrophobic solutes,[23] and also in hydration water of proteins[24] and micelles.[25] The anomalous diffusion is a consequence of the confinement leading to highly structured water, in which a water molecule has a reduced choice of escaping and overtaking

its neighbors. It is to remember that in the extreme case of single file diffusion, where the particles cannot cross each other, the value of α is 0.5. However, we obtain the overall diffusion coefficient from a linear fit of the full MSD data as calculated from simulation trajectory as well as from the integral of velocity correlation function (VCF) (discussed later). Diffusion coefficients in the parallel direction of the plates have also been calculated from the slope of the $<\Delta r_{||}^2(t)>$ vs. t plot and from the integral of the VCF as obtained by projecting velocities in the xy-plane parallel to the plates. Larger value of the $D_{||}$ as compared to the overall diffusivity D signifies that the diffusion along the direction perpendicular to the plate is severely damped. Diffusion coefficients as listed[26] in Table II indicate faster diffusion in case of a_0 = 6 Å plate as compared to the other two cases. The larger intermolecular distance (a_0) within the plate dilutes the dispersion interaction between the plate and water and has depleting effect on the water structure. Thus, faster translational dynamics of water in the intersolute region of the plate with larger a_0 value can be justified in the context of excess entropy scaling of the dynamical quantities.[27]

The velocity correlation function (VCF) has also been calculated for all the three plates using Eq. (1) with f_i replaced by velocity of particle i i.e v_i and are shown in Fig. 6(a). As in the case of MSDs, the VCF of the water molecules confined between the two plates also changes with intermolecular distance (a_0) within the plate. The VCF of the confined water molecules in the interplate region of the plates with a_0 = 6 Å is the least structured and is very similar to that (not shown for clarity) of the bulk water molecules. As the intermolecular distance a_0 within the plate decreases from 6 to 5 and then to 4 Å, a significant change in the corresponding VCF with more undulating structures has been observed. The undulating structure with negative value of the VCF is a consequence of caging effect and rebounding of the water molecule by the surrounding environment. The quantitative difference among various VCFs is better manifested when diffusion coefficient D of the water molecules is calculated from the

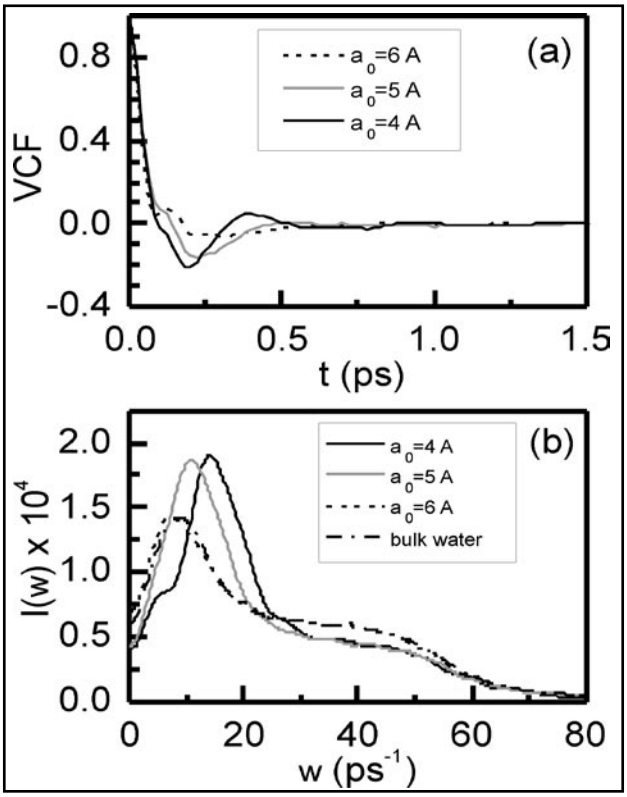

***Figure** 6: (a) Velocity-velocity autocorrelation functions (VCF) for the water oxygens in the confined region for the three different plate-water systems. (b) Power spectra obtained from the Fourier transform of the velocity-velocity autocorrelation functions for the water oxygens in the confined region.*

TABLE II: Diffusion coefficients of water for different solute-water systems as calculated from MSD as well as VCF

	D ($cm^2 sec^{-1}$)		$D_{||}$ ($cm^2 sec^{-1}$)	
a_0 (Å)	MSD	VCF	MSD	VCF
4.0	1.65	1.70	2.37	2.82
5.0	1.94	1.84	2.75	2.99
6.0	2.24	2.47	3.12	3.64

integral of the VCF. The diffusivities of confined water for different plates as obtained from the integration of the VCFs upto 2 ps are tabulated in Table II along with those obtained from MSDs.

Further comparison of the collective vibrational frequencies of the confined water molecules for different plate-water systems can be made by calculating power spectrum as obtained from the Fourier transform of the VCF for a plate-water system. The power spectra for

three different plate-water systems and that of the bulk state are presented in Fig. 6(b). The frequency spectrum for the bulk water (see dash-dot line in Fig 6(b)) has the characteristic major peak around 9 ps^{-1}, attributed to manybody motions and a broad shoulder-like peak at around 30-45 ps^{-1}, attributed to pairwise intermolecular oxygen-oxygen vibrations. The frequency spectrum for a_0 = 6 Å plate-water system as shown by the dashed line is quite similar to that (dash-dot line) of the bulk water. However, the same for a_0 = 5 (dotted line) or 4 Å (black solid line) is quite different from that of the bulk water. In these two cases, where paraffin molecules are slightly closely packed (as compared to a_0 = 6 Å case), the first peak of the spectrum is shifted to higher frequency and the amplitude is also higher. In case of a_0 = 4 Å plate-water system, apart from the shift of peak frequency to around 14 ps^{-1}, a small shoulder appears near 5-6 ps^{-1} (see black line). For a_0 = 4 or 5 Å case, the amplitude of the shoulder region around 30-45 ps^{-1} is slightly reduced as compared to the same for bulk or a_0 = 6 Å case. This indicates that in these two cases contribution of the multi-body vibrations dominates over that from pairwise intermolecular vibrations. The frequency distribution as shown in the power spectrum is a measure of the relative population of the density of states of independent oscillators of a particular frequency, which in turn is related to the local motions of water molecules. The shift of the main peak to higher frequency in case of a_0 = 4 or 5 Å case is a consequence of the larger force acing on the water molecules in the given environment. Similar behavior of the power spectrum has been observed in earlier investigations.[22]

When water meets a hydrophobic surface: effect of surface topology

Knowledge of the behavior of water in contact with single nanoscopic hydrophobic surface is of immense importance in the context of wetting/dewetting of the surface. In addition it also helps us to understand the mechanism of dewetting in the intersolute region. We intend to study the hydration behavior of single paraffin-like plate to examine whether any correlation exists between the structure of water adjacent to single surface and the observed dewetting in the intersolute region. In other words, we are interested to know whether the dewetting in the intersolute region stems from dewetted interface between single solute and water. We also investigate the effect of surface topology that dictates the hydrophobicity of the surface on the spatial as well as orientational structure of water near the surface. Here we have considered 4 different types of paraffin like plates with a_0 values 4, 5, 6 and 7 Å. The normalized one-particle density profiles $\rho(z)/\rho_0$ of water around the four types of hydrophobic plates as obtained from the MD simulation have been shown in Fig. 7 (a) and the corresponding instantaneous density profiles have also been shown in Fig. 7(b). It is clear from both the figures that the average density of water near the solute surface is quite high in all the cases and instantaneous density does not show any large fluctuation, indicating a stable layer of water molecule adjacent to the solute surface.

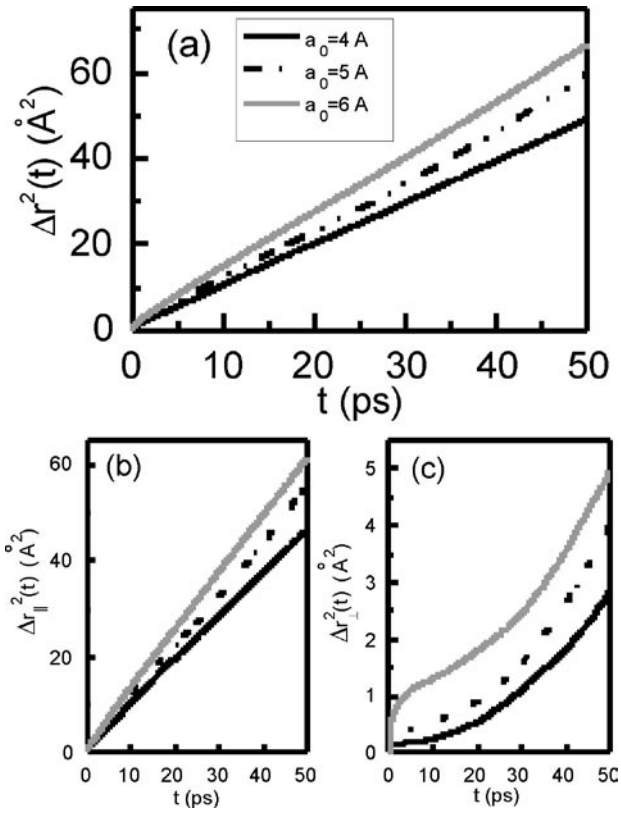

Figure 7: *The normalized single particle Density $\rho(z)/\rho_0$ of water oxygen in and around three different plates with intermolecular spacing (a) a_0 = 4 Å (b) 5 Å and (c) 6 Å and (d) 7 Å.*

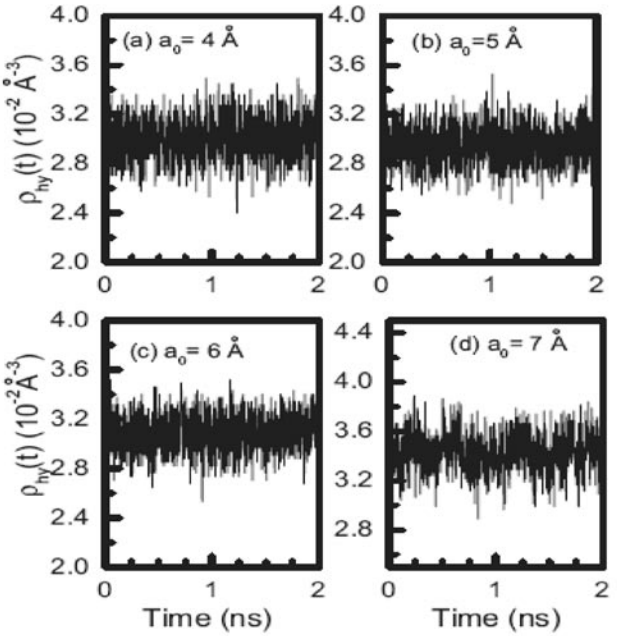

***Figure** 8 : Plot of the instantaneous number density of water, $\rho_c(t)$ in the intersolute region corresponding to Fig. 7*

In case of a_0 = 7 Å plate, a small peak appears at a distance below 2.5 Å, which is not observed in any of the other cases. Appearance of this small density peak in the excluded volume region of the plate (see Fig. 7(d)) is a consequence of protrusion of water molecule in the intermolecular space of the paraffin plate. This is clearly seen in Fig. 9(d), where individual paraffin molecule in the plate is completely hydrated. It is interesting to point out that one of the central issues in hydrophobic dewetting at the large length scale is the issue of correlation between the structure of water at the single solute-water interface with the same in the intersolute region. It has been posited[10,11] that when a large hydrophobic solute is immersed in water, due to depletion of hydrogen bond of the water molecules near the solute surface, a liquid-vapor interface is created and when two such solutes come close to each other below a critical distance, the fluctuation in the individual solute-water interface induces dewetting in the intersolute region. In the present study we found a dewetted intersolute region between two plates with a_0=6 Å (see Figs. 3(c) and 4(c)). Thus, according to the above proposition a vapor-liquid interface should exist when single plate is immersed in water. However, our analysis of average density in the vicinity of single plate

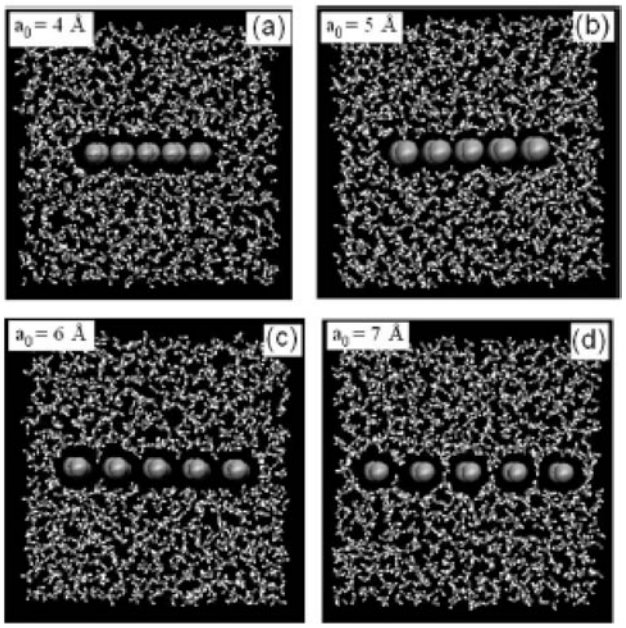

***Figure** 9: Snapshots of the paraffin-water systems at 2 ns for the four different plate-water systems. The plates with intermolecular spacing of (a) a_0=4 Å, (b) a_0=5 Å, (c) a_0=6 Å, and (d) a_0=7 Å have been shown. The water molecules from front and the back sides of the plates have been removed for clarity.*

with a_0=6 Å shows a completely wet state with high density of water adjacent to the plate surface (see Fig. 7(c)) and the instantaneous density (see Fig. 8(c)) also does not show any large fluctuation. Therefore, it can be concluded that dewetting in this case is a consequence of the combined effect of the two plates, not originated from the individual plate-water interfacial (dewetted) structure.

A. Hydrogen bonding of water

It is generally believed that breaking of hydrogen bonds near a hydrophobic surface is the guiding factor for the stability of water at the interface. A water molecule in the bulk forms on an average three to four hydrogen bonds, while near a nonpolar surface, hydrogen bonds of water molecules are broken due to the unavailability of neighboring water molecules. In order to investigate the effect of plate topology on the hydrogen bonding of water, number of hydrogen bonds per water molecules, n_{HB}, has been calculated for each of the plates and is shown in Fig. 10. A depletion region in the vicinity of the plate, where number of hydrogen bonds are less than that in the bulk.

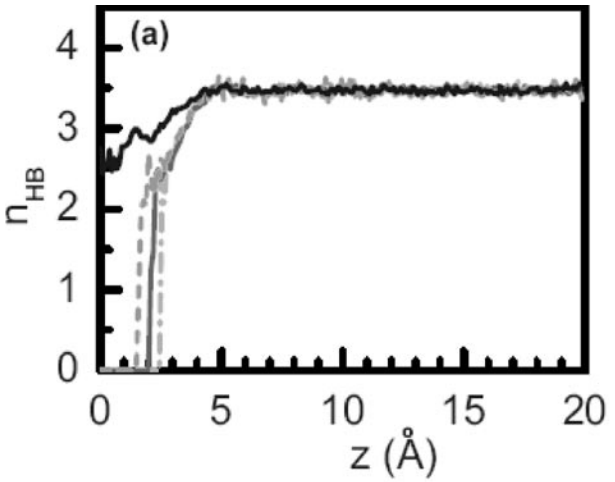

Figure 10: *Number of hydrogen bonds n_{HB} per water molecules as a function of perpendicular distance z from the solute plate for four different paraffin-like plates with intermolecular spacings a_0=4 Å (dash-dot), a_0=5 Å (light black line), a_0=6 Å (dashed light gray line) and a_0=7 Å (black line).*

It is interesting to observe that nonzero numbers of hydrogen bonds are found up to different critical distance of approach to the plate surface for different plates. The critical distances in which nonzero hydrogen bonds of water molecules are found is lesser for plates with smaller a_0 values. In the case of plate with a_0=7 Å, however, there are hydrogen bonded molecules even at the interior of the plate, since in this case water molecules are present in the intermolecular region of the plate.

B. Orientational structure of water

The orientational structure of the water molecules has been analyzed by calculating orientational probability distributions $P_\mu(\cos\varphi)$ and $P_{OH}(\cos\theta)$ of the water molecules. The angles φ and θ in the above two cases respectively are the angles made by the dipole moment vector μ and the OH bond vector of the water with the outward normal from the plate pointing into the water. To observe how model water molecules orient themselves adjacent to the plate, we have considered four different layers of water molecules around the plate. Layer 1 is considered to be the layer of water molecules closest to the outside surfaces of the plate, in which water molecules are in the repulsive solute-water interaction region corresponding to the low-

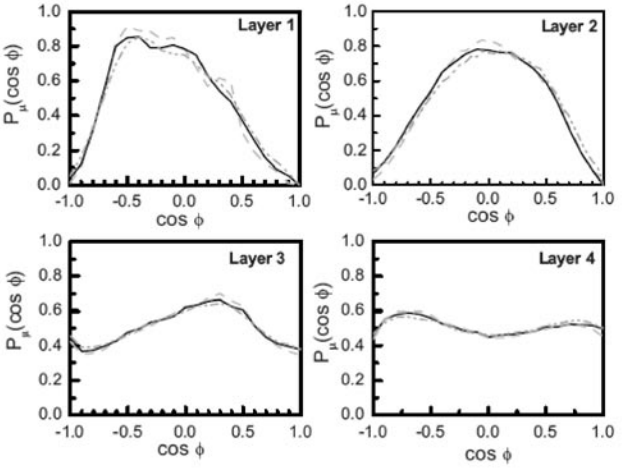

Figure 11: *(a): Orientational distributions of the dipole moment vector, $P_\mu(\cos\varphi)$ for 3 different plates for water in the four different layers.*

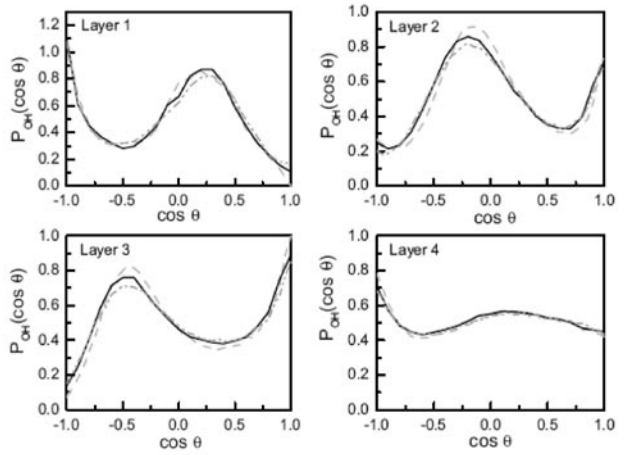

(b) Orientational distributions of the OH bond vector, $P_{OH}(\cos\theta)$ for three different plates for water in the four different layers around the hydrophobic plate.

density edges before the first density maximum of the density profile. Layer 2 incorporates water molecules corresponding to the first major density peak near the plate surface, while layer 3 corresponds to the trough between first and second density peaks and layer 4 is the region where molecules contributing to second density maximum reside. In order to investigate the effect of the plate topology on the orientational distributions, we have presented $P_\mu(\cos\varphi)$ of the water molecules in the four different layers around the plate for each of the four plates with a_0=4, 5, and 6 Å in Fig.11(a). The dipole moment distributions of water in layer 1 around different plates show a broad distribution with major peak of the distribution at around 120°

for the plate with a_0=4 Å. In layer 2 the water molecules show a broad distribution around 90°, whereas in layer 3 the peak of the distribution is around 72°. In the layer 4, the distribution is almost flat and around 0.5, which is characteristic of bulk water molecules. Effect of solute topology is not so prominent in this case. Similar analyses have been considered[9,20,28] for water near other nonpolar solute surfaces.

The distributions for the OH bond vector for the four layers of water have been shown in Fig. 11(b). Here the orientation of the OH bond in each layer for the three different plates with a_0=4, 5, and 6 Å shows almost similar behavior in all four layers, showing a very little effect of the topology of the plate on the orientations of the water molecules around it. In the layer 1 the OH distribution has two peaks at around 75° and 180°. The distribution in the layer 1 indicates that a large fraction of water molecules orient themselves with one OH bond pointing directly toward the hydrophobic surface as seen in the earlier simulations of Lee et al.[28] In layer 2 the distribution has peaks at around 80° and 0°, whereas in layer 3 the peaks of the distributions are at 115° and 0°.

Concluding Remarks

Multifaceted nature of hydrophobicity at the nanoscale has been observed through disparate manifestations of the behavior of water in the intersolute region. Although effect of solute dispersion interaction has been studied[9,14] earlier, in the present study it has been demonstrated that by tunning the intermolecular spacing of the solute plate, keeping individual solute-water interaction unchanged, the manifestation of hydrophobicity can be regulated to achieve any of the wet, dry and intermittent wet-dry states. The present study thus reconciles conflicting observations made in earlier experimental and theoretical studies in a single context. The topology of the extended hydrophobic solute has been shown to have considerable effect on the dynamics of confined water as well. It is interesting to observe that a slight change in topology (~1 Å change in the intermolecular spacing) of the model hydrophobic plate modifies translational and vibrational dynamics of confined water molecules so significantly. The nature of the translational dynamics has been shown to be anomalous. The translational diffusivity of the confined water molecule decreases with decreasing a_0 values. The effect of the intermolecular distance within the paraffin plate on the vibrational spectrum is also significant. The present results also establish a link between the phenomenon of dewetting observed[25] in case of a_0 = 6 Å plates with the fast dynamics of interplate water for the same plate in a state, which is a precursor to the dewetted state. The present study, therefore, clearly demonstrates that the structural and dynamical characteristics of the intersolute water depend on the minute details of the solute.[26] The present observation can be used to tailor new materials with required wettability and channels with desired water accessibility and also help to understand the environment near a protein surface.

Acknowledgments

It is a pleasure to thank Dr. Swapan K Ghosh and Dr. T. Mukherjee for their interest and encouragement.

References

1. W. Kauzmann, *Adv. Protein Chem*. **14**, 1 (1959).
2. C. Tanford, *The Hydrophobic Effect: Formation of Micelles and Biological Membranes*; John Weiley: New York, 1973.
3. H. S. Ashbaugh and L. R. Pratt, *Rev. Mod. Phys*. 78, 159 (2006).
4. P. Ball, *Nature* **423**, 25 (2003).
5. P. Ball, *Chem PhysChem* **9**, 2677 (2008).
6. D. Chandler, *Nature* **437**, 640 (2005).
7. A. Wallqvist and B. J. Berne, *J. Phys. Chem*. **99**, 2893 (1995).
8. X. Huang, C. J. Margulis and B. J. Berne, *Proc. Natl. Acad. Sci. U.S.A*. **100**, 11953 (2003).
9. N. Choudhury and B. M. Pettitt, *J. Am. Chem. Soc.* **127**, 3556 (2005).
10. K. Lum, D. Chandler and J. D. Weeks, *J. Phys. Chem. B* **103**, 4570 (1999).
11. F. H. Stillinger, *J. Solution Chem*. **2**, 141 (1973).
12. G. Hummer, J. C. Rasaiah and J. P. Noworyta, *Nature* **414**, 188 (2001).
13. T. Koishi, S. Yoo, K. Yasuoka, X. C. Zeng, T. Narumi, R. Sasukita, A. Kawai, H. Furusawa, A. Suenaga, N. Okimoto, N. Futatsugi and T. Ebisuzaki, *Phys. Rev. Lett*. **93**, 185701 (2004).
14. N Choudhury and B. M.Pettitt, *J. Am. Chem. Soc*. **129**, 4847 (2007).
15. P. Liu et al. *Nature 437*, 159 (2005).

16. R. Zhou, X. Huang and C. J. Margulis and B. J. Berne, *Science*, **305**, 1605 (2004).
17. H. J. C. Jorgensen, J. D. Madura, and C. J. Swenson, *J. Am. Chem. Soc*. **106**, 6638 (1984).
18. N. Choudhury, *J. Phys. Chem*. B **112**, 6296 (2008).
19. Y. Zubavicus and M. Grunze, *Science*, **304**, 974 (2004). P. Wernet, D. Nordlund, U. Bergmann, M. Cavalleri, M. Odelius, H. Ogasawara, L. A. Naslund, T. K. Hirsch, L. Ojamae, P. Glatzel, L. G. Pettersson and M. A. Nilsson, *Science* **304**, 795 (2004). C. P. Schultz, *Nat. Struct. Biol*. 7, 7 (2000). A. Troullier, D. Reinstadle, Y. Dupont, D. Naumann and V. Forge, *Nat. Struct. Biol*. 7, 78 (2000).
20. O. Beckstein and M. S. P.Sansom, *Proc. Natl. Acad. Sci. USA*, **100**, 7063 (2003).
21. P. Liu, E. Harder and B. J. Berne, *J. Phys. Chem. B* **108**, 6595 (2004).
22. N. Choudhury and B. M. Pettitt, *J. Phys. Chem. B* **109**, 6422 (2005).
23. N. Choudhury, *J. Phys. Chem. C* **111**, 2565 (2007).
24. A. R. Bizzarri and S. Connistraro, *J. Phys. Chem. B* **106**, 6617 (2002).
25. B. Bagchi, *Chem. Rev*. **105**, 3197 (2005).
26. N. Choudhury, *J. Chem. Phys.* **132**, 064505 (2010).
27. M. Dzugutov, *Nature* (London) **381**, 137 (1996).
28. N. Choudhury, *J. Chem. Phys.* **131**, 014507 (2009).

Dr. Niharendu Choudhury *received his M. Sc. Degree in Physical Chemistry from Jadavpur University, Calcutta. He joined BARC in 1991 through 35th batch of the BARC Training School and received Homi Bhabha Award in 1992. He obtained his Ph.D. degree in Chemistry from Bombay University in 2000 for his work on "Density Functional Theory of Macroscopic Systems". He has spent two years (2003-2005) as a postdoctoral fellow at Chemistry Department of University of Houston, Houston, TX, USA. Dr. Choudhury is associated with various research areas encompassing development of classical density function theory and integral equation theory and application of molecular dynamics simulation to investigate structure and dynamics in the condensed phase. In particular, he is involved in the study of structure and dynamics of fluids in bulk as well as in nano-confined geometries. Special emphasis of his research has been to understand hydrophobicity at the nanoscale and its role in macromolecular self-assembly processes such as protein folding, aggregation of hydrophobic nanoparticles in aqueous solution.*

Studies on Dissociation Dynamics and Kinetics: Theoretical Inputs to Experimental Work

Awadhesh Kumar, Hari P. Upadhyaya, Prakash D. Naik
Radiation & Photochemistry Division, Bhabha Atomic Research Centre, Trombay, Mumbai – 400 085

Abstract

The article demonstrates a synergistic relationship between experimental and theoretical results in understanding the photodissociation dynamics and kinetics of atmospherically-relevant polyatomic organic molecules. The dynamics of formation of OH, an environmentally important radical (aptly known as atmospheric scavenger), is investigated. Not only molecules containing OH group (such as carboxylic acids) generate OH on UV laser excitation, but those devoid of OH (such as cyclic ethers) also produce OH after intramolecular re-arrangement. The temperature-dependent kinetics of OH with various organic pollutants has also been discussed.

Introduction

Experiments and theory are many times complementary to each other in providing a holistic picture of a chemical process. Theory is an important tool for rationalization and validation of experimental results. A suitable marriage between experiment and theory provides clear understanding of a molecular system under investigation. Sometimes experiments are too complex and difficult to perform or interpret, and in such cases theory becomes very convenient to predict the observables. At the same time for any new theoretical model proposed, an experimental demonstration is a final proof for the theory. We have employed theory to support and complement our experimental results on dissociation dynamics and kinetics of some important polyatomic organic molecules of atmospheric importance. Structures and energies of various molecular species in an elementary reaction are calculated using molecular orbital (MO) theory with the Gaussian routine [1]. One of the important aspects of dissociation dynamics is to measure partitioning of the available energy in various degrees of freedom of the photofragments. The measured energy release in the products is modeled using theoretical models of energy partitioning, such as statistical, impulsive and hybrid. The observed time evolution of a product is compared with a unimolecular statistical rate theory, Rice-Ramsperger-Kassel-Marcus (RRKM). The RRKM theory also predicts the branching ratio of two dissociation pathways, and thus can be compared with the measured values.

The main objective of the work is to understand dynamics and kinetics of some atmospherically important organic molecules. An interest in dissociation dynamics of polyatomic molecules has been to investigate various dissociation channels operating from the ground and the excited electronic states, and to measure partitioning of the available energy among various degrees of freedom of photoproducts. Our work in kinetics is focused on accurate measurements of temperature-dependent rate coefficients of OH and Cl with various organic pollutants, and to estimate the atmospheric life times of these pollutants to assess their environmental impact. These measurements can provide a tool to find out a correlation between structure and reactivity of a molecule. We have employed a laser photolysis-laser induced fluorescence (LP-LIF) technique to study the dynamics and kinetics of interest. In addition to LIF, we have also used resonance-enhanced multiphoton ionization (REMPI), a more sensitive and versatile diagnostic, to probe a transient in a collision-free condition for a better understanding of the dynamics taking place at a molecular level. This technique is complementary to LIF, since it does not require a molecule to fluoresce for detection. However, the REMPI results are not discussed in this article.

We report experimental studies on dynamics of the C-OH bond dissociation, leading to OH formation, from carboxylic acids, cyclic ethers and acetyl acetone on UV excitation at 193, 248 and 266 nm.These experimental results have been substantially corroborated through theoretical inputs. Similar theoretical support to measurements on kinetics of a few important organic molecules with OH, a radical of atmospheric importance, has been discussed.

Results And Discussion

A. Photodissociation dynamics

1. Carboxylic acids

W have investigated dynamics of the C-OH bond dissociation in both saturated and unsaturated carboxylic acids [2,3], such as acetic acid, difluoroacetic acid, thiolactic acid, acrylic and propiolic acids. The principal objective was to find out whether an important feature of potential energy surface, i.e. an exit barrier, is present in the C-OH bond dissociation channel of carboxylic acids (reaction 1). If an exit barrier is present, how does it influence the dynamics of dissociation of carboxylic acids, particularly the partitioning of the available energy between photofragments?

$$RCO_2H \longrightarrow RCO + OH \qquad (1)$$

LIF detection of the nascent OH radical and measurement of its fluorescence excitation spectra provide all the information on the translational and internal state distribution (vibration, rotation, spin-orbit and Λ-doubling components) of the OH fragment. A typical LIF excitation spectrum of OH produced on photoexcitation of propiolic acid ($HC\equiv C\text{-}CO_2H$) is shown in Fig.1. These measurements reveal that, on photoexcitation of carboxylic acids, OH is produced mostly vibrationally cold (v″=0), with moderate rotational excitation, which is characterized by a rotational temperature of 600-1700 K. In unsaturated acrylic and propiolic acids, the OH fragment is also detected in v"=1 (<5%), mainly because of a greater yield of OH. But, an appreciable fraction of the available energy, that is f_T, is partitioned into the relative translation of

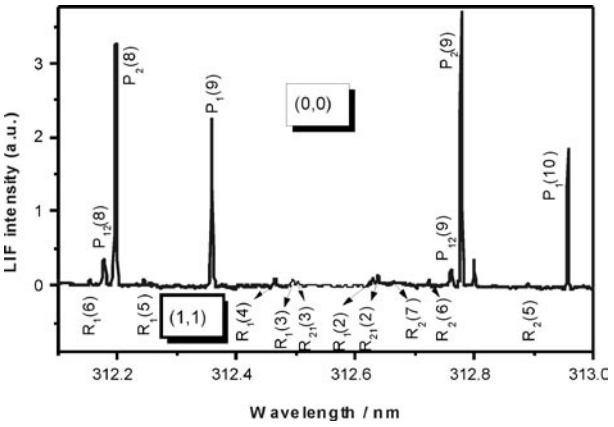

Figure 1: *A typical LIF excitation spectrum of the (0,0) and (1,1) bands of OH (A-X) produced on photoexcitation of propiolic acid (20 mTorr, 50 ns time delay between pump and probe lasers) at 193 nm. Rotational lines are marked in the figure.*

the fragments, with the f_T values varying from 0.30 to 0.75, in the photodissociation of carboxylic acids. Relatively greater f_T values are observed in unsaturated carboxylic acids.

Since a significant fraction of the available energy is released in the relative translation of the products, either the OH channel occurs impulsively from a repulsive state of a carboxylic acid, or it has an exit barrier. The impulsive C-OH bond dissociation should lead to fast formation of OH, within the photolysis laser pulse of 20 ns. But, we observed relatively slow formation of OH with a rate coefficient of $\leq 9.0\text{x}10^6$ s^{-1}. Moreover, an impulsive model of energy partitioning, applicable for the dissociation from a repulsive state, does not explain the measured energy in the fragments. Thus, the second possibility of the presence of an exit barrier in the C-OH bond scission, producing OH, can be responsible for a high amount of energy in the relative translation. This prediction is supported by modeling the measured partitioning of the available energy in the fragments by a hybrid model. The available energy partitioned to the fragments in a dissociation process with an exit barrier is explained well with a hybrid model of energy partitioning, which is a combination of both the statistical and impulsive models. In this model, the exit barrier energy and the energy above the barrier are treated impulsively and statistically, respectively. A dissociation process

with a barrier occurs generally from an excited electronic state, since dissociation from the ground electronic state is barrier-less for stable molecules. This mechanism is validated through our theoretical calculations, which show the presence of an expected exit barrier in an excited electronic state; and corresponding transition state (TS) structures have been characterized. The excited state calculations at the CIS/6-311+G(d,p) level reveal that the initially excited state is not repulsive. These calculations rule out dissociation from a repulsive state, and suggest an exit barrier in the C-OH channel. Thus, experimental results are validated by theoretical results.

The initial excitation of a carboxylic acid at 193 nm populates the S_1 or the S_2 state, which relaxes to the lower state T_1 by radiative and/or non-radiative processes and subsequently dissociates involving the C-OH bond cleavage to generate OH. However, thiolactic acid, containing a –SH functional group at the α position to the –COOH group, dissociates from the S_1 state ($\pi^*_{CO} \leftarrow n_S$) after excitation at 193 nm. This influence of the lone pairs of electrons on the S atom is not observed for the F atoms in difluoroacetic acid, which dissociates from the T_1 state ($\pi^*_{CO} \leftarrow n_O$). Theoretical characterization of the dissociating state of propiolic acid to be T_1 ($\pi^*_{C\equiv C} \leftarrow \pi_{C\equiv C}$), explains much of our experimental results, such as the observed higher fraction of the available energy into the relative translation (due to the presence of an exit barrier on the T_1 surface), slow formation of OH (attributed to a slow intersystem crossing to the dissociating state T_1) and a preferential population of the $^2\Pi_{3/2}$ spin orbit state (due to the triplet nature of the dissociating state).

In addition to the OH channel, decarboxylation and decarbonylation channels have also been investigated. Our experimental results, combined with the reported literature on photodissociation of carboxylic acids, suggest that CO_2 and CO are formed from the dissociation of the highly vibrationally excited ground electronic state on excitation at 193 nm. We have characterized TS for their formation from the ground electronic state of carboxylic acids. Decarboxylation of propiolic acid is a unimolecular reaction channel involving

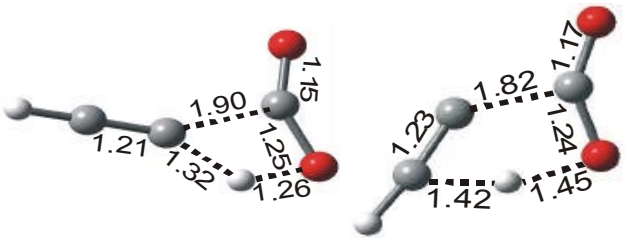

Figure 2. *The figure depicts transition state structures (four- and five-centred) for decarboxylation channels from propiolic acid. Bond distances are marked in angstrom. Structures are optimized at B3LYP/6-311++G(d,p) level of theory.*

a concerted mechanism with four-centred TS, which is nearly planar with the hydroxyl proton adopting the trans conformation with respect to the carboxyl group. The most stable s-cis conformer changes to the s-trans conformer, before undergoing decarboxylation reaction. But, in addition to the reaction mechanism involving a four-centred TS, decarboxylation via five-centred TS is also probable. The four- and five-centred TS structures for decarboxylation channels from propiolic acid are depicted in Fig. 2. The five-centred TS structure is perfectly planar. In comparison to the four-centred TS, the dissociating C-C bond is extended less, but the O-H bond is extended more to enable the H atom reach the target C atom. Both the decarboxylation reactions in propiolic acid have a comparable activation barrier, with slightly lower for the four-centred reaction, and hence, expected to be equally probable (assuming the similar frequency factor). The relative importance of these decarboxylation channels has been calculated using RRKM unimolecular rate theory. The unimolecular rate coefficient, k(E) is given by

$$k(E) = \frac{\sigma}{h} \frac{w^{\#}(E - E^{\#})}{\rho(E)} \qquad (2)$$

where h is the Planck's constant, σ is the symmetry factor, $w^{\#}(E\text{-}E^{\#})$ is the total number of the states and ρ(E) is the density of the states of the reactant. The RRKM statistical theory predicts CO_2 formation via the four-centred concerted mechanism to be faster by a factor of two, and hence contributing more to the yield.

However, unlike other carboxylic acids, for which the formation of CO is reported to be a

primary reaction, in propiolic acid it occurs in two steps with a very small activation barrier (~3 kcal mol^{-1}) for the second step. First, 1,2-OH migration takes place (reaction 3a), and then subsequently CO is produced after the C-C bond cleavage (reaction 3b).

$$HC{\equiv}C\text{-}COOH \rightarrow HC{=}C(OH)CO \quad (3a)$$

$$HC{=}C(OH)CO \rightarrow HC{\equiv}COH + CO \quad (3b)$$

The first step involves an asymmetrical three-centred TS having a non-planar geometry, with the new C-OH bond shorter (1.74 Å) than the breaking one (1.92 Å). The C≡C bond is lengthened, whereas the C-C bond is shortened in the TS. The dihedral angle CCOH of 93.4° implies that OH moves from the planar ground state geometry to acquire a perpendicular orientation with respect to the C atoms with which it is attached in the TS. After the migration of OH, an intermediate with a planar geometry is generated. Both the C≡C and the C-C bonds acquire double bond characters with almost the same lengths (1.34 and 1.36 Å). In the second step, the intermediate undergoes the C-CO bond cleavage to generate CO via TS with a planar geometry and the C-CO bond lengthened to 1.71 Å.

Between two molecular pathways of CO_2 and CO elimination from propiolic acid, the lower energy pathway is predicted to be CO_2 elimination with an activation barrier (E_b) of 59.8 and 60.9 kcal mol^{-1} for the four- and the five-centred concerted mechanisms, respectively. The CO elimination is the higher energy channel. Based on these calculations, we expect CO_2 to be produced in a higher yield than CO.

2. Cyclic ethers

The photodissociation of cyclic ethers [3,4], such as tetrahydropyran, tetrahydrofuran, styrene oxide, 1,3-butadiene monoxide and morpholine, at 193 nm produces the OH radical. This OH channel is unexpected, since these molecules are devoid of any OH functional group. The proposed mechanism for OH formation, based on experimental and theoretical results, involves first relaxation of the electronically excited cyclic ether to its vibrationally excited ground electronic state. Subsequently, the ring opening occurs by cleavage of the C-O bond, with simultaneous 1,3-H atom migration to the O atom (singlet pathway) or the C-O bond scission generating a triplet biradical, followed by H atom migration to the O atom (triplet pathway). With these intramolecular re-arrangements, the molecule acquires an OH group, and subsequent C-OH bond scission produces OH. In the case of styrene oxide and 1,3-butadiene monoxide, which have asymmetrical C-O bonds, the ring opening occurs by cleavage of either of the two non-equivalent C-O bonds (α- and β- with respect to the ethylene or phenyl group), generating 1,3-biradicals, which isomerize to enols. Between α- and β-C-O bond cleavages, the former has a preference because of greater stability of the corresponding biradical produced. The enols, in turn, undergo either simple C-OH bond cleavage, producing the OH radical, or get converted to their more stable keto forms. Both these channels from enols are observed experimentally. However, OH was not observed from other simple oxiranes, ethylene and propylene oxides, under similar conditions, which is attributed mainly to their lower absorption cross-sections at 193 nm.

3. Acetylacetone

Theoretical calculations have provided sufficient support to our experimental results on UV photodissociation of acetylacetone (H_3C–CO–CH_2–CO–CH_3) [5] as well in understanding its dynamics of dissociation leading to OH formation. Like cyclic ethers, acetylacetone also lacks an OH group, but generates OH on excitation at 193, 248 and 266 nm. The OH channel operates from its enolic form, H_3C–COCH=C(OH)–CH_3, which is predominant in the gas phase. The average translational energy partitioned into the photofragments is found to be 16.0±4.0, 17.3±4.2 and 19.2±4.7 kcal/mol at 266, 248, and 193 nm excitation, respectively. Since the translational energy released is almost independent of the excitation energy, the C-OH dissociation channel should have an exit barrier. Detailed ab initio calculations, using configuration interaction-singles method, suggest acetylacetone is initially prepared in the $^1(\pi\pi^*)$ state at 266 and 248 nm excitation, and the OH fragment is produced from

the lowest $^3(\pi\pi^*)$ state. However, upon excitation at 193 nm, the initially prepared Rydberg state of acetylacetone crosses over fast to the nearby σ* repulsive state along the C–OH bond, and dissociates to give the OH radical.

B. Kinetics of atmospherically important organic molecules with OH

The OH radical reacts with an organic molecule by generally abstracting one H atom. A molecule containing unsaturation undergoes an additional reaction with OH that is an addition reaction. The rate coefficients of OH with unsaturated alcohols (allyl, H_2C=CH-CH_2OH, and propargyl, HC≡C-CH_2OH, alcohols) have been measured to be $3.7x10^{-11}$ and $9.2x10^{-12}$ molecule^{-1} cm^3 s^{-1}, respectively. The detailed mechanism of OH attack on the unsaturation centre was understood with theoretical calculations. The OH addition reaction can be initiated with its attack on either the α-C atom or β-C atom to the CH_2OH group. Theoretical calculations of structures and energies suggest preference for attack on the α-C atom, and the relative reactivity of these alcohols could be understood in terms of HOMO-LUMO energy gap.

Kinetics of reaction of the OH radical with morpholine has been investigated in the temperature range of 298-363 K, using laser photolysis-laser-induced fluorescence technique [6]. The rate constant at room temperature k(298) is $(8.0 \pm 0.1)x10^{-11}$ molecule^{-1} cm^3 s^{-1}. The rate constants are greater compared with those of similar heterocyclic molecules with oxygen atom, but comparable to those reported for aliphatic amines. The rate constant decreases with temperature in the range studied, suggesting formation of a prereactive complex. Ab initio molecular orbital calculations support the experimental results by predicting the formation of prereactive complexes, 5-7 kcal mol^{-1} (shown in Fig. 3) lower in energy as compared with the reactants, due to hydrogen bond interaction between OH and the N/O atom of morpholine. The stability of the complex involving the nitrogen atom is found to be more than that involving the oxygen atom. The optimized TS structures and energies for the different pathways of hydrogen abstraction from these prereactive complexes explain the observation of negative activation energy.

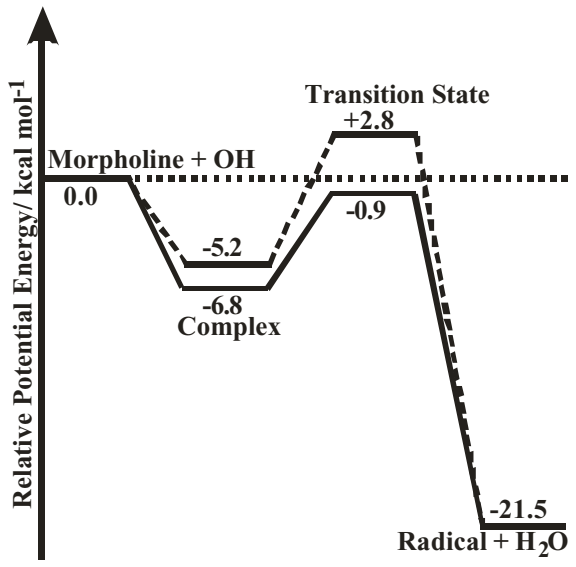

Figure 3 : *Potential energy curves for reactions of morpholine with OH; dashed and solid lines represent complexes of OH with O and N atoms, respectively. Transition states for H_2O elimination channels are depicted.*

Conclusions

We have presented some of our experimental results on photodissociation dynamics and kinetics of polyatomic organic molecules, and discussed how the theoretical inputs have aided in understanding the physico-chemical processes occurring at a microscopic level. For an example, detection of OH in photodissociation of cyclic ethers, which are devoid of any OH group, was difficult to explain without resorting to molecular orbital calculations, which predicted an intramolecular re-arrangement preceding the C-OH bond scission to produce OH. The pivotal role of theory in understanding experimental results can be summarized by quoting R. Hoffmann, who opined that "The most important role for theory in chemistry is to provide a framework in which to think and organize knowledge; and the peculiar feature of theory is that it generally trails experiments, and yet experiment cannot survive without it."

References

1. Frisch, M. J.; Trucks, G. W.; Schlegel, H. B.; et al.; 1992 ed.; 92, G., Ed.; Gaussian, Inc.: Pittsburgh, PA, 1992.

2. P.D. Naik, Hari P. Upadhyaya, Awadhesh Kumar, A.V. Sapre and J.P. Mittal, *J. Photochem. Photobiol*. C 3 (2003) 165.
3. P.D. Naik, Awadhesh Kumar, Hari P. Upadhyaya, P.N. Bajaj and S.K. Sarkar, Laser Induced Fluorescence Spectroscopy, in *Lasers in Chemistry*; Lackner, M., Ed.; Wiley-VCH Publications, 2008; Vol. 1; pp 463.
4. Sumana SenGupta, Awadhesh Kumar, P.D. Naik, P.N. Bajaj, *Chem. Phys. Lett*. 465 (2008) 197.
5. Hari P. Upadhyaya, Awadhesh Kumar and Prakash D. Naik *J. Chem. Phys*. 118 (2003) 2590.
6. Sumana SenGupta, Yogesh Indulkar, Awadhesh Kumar, Suresh Dhanya, P.D. Naik and P.N. Bajaj, *J. Phys. Chem. A* 114 (2010) 7709.

Awadhesh Kumar *was born in 1964 in Bihar, India. He received his BSc in Chemistry in 1985 from University of Delhi, India and MSc in Chemistry in 1987 from Indian Institute of Technology, Kanpur, India. He is currently working as a Scientific Officer in Radiation & Photochemistry Division of Bhabha Atomic Research Centre, Mumbai, India. He received his Ph.D. degree in Chemistry from University of Mumbai in 1995. He worked for a period of 2 years at National Tsing Hua University, Hsinchu, Taiwan with Prof. Yuan Pern Lee. His current research interests focus on dynamics of gas phase reactions induced by lasers using resonant four-wave mixing and laser-induced fluorescence with special reference to atmospherically important free radical species.*

Hari P. Upadhyaya *was born in 1965 in Guwahati, India. He received his B.Sc. in Chemistry in 1987 from North Eastern Hill University, Shillong, India and M.Sc. in Chemistry in 1990 from University of Delhi, India. He is currently working as a Scientific Officer in Radiation & Photochemistry Division of Bhabha Atomic Research Centre, Mumbai, India. He worked for a period of 1 year at Institute of Physical Chemistry, University of Heidelberg, Germany in the area of photodissociation and reaction dynamics with Prof. J. Wolfrum during 1997–1998. Subsequently, he received his Ph.D. degree in Chemistry from University of Mumbai in 2001. In his post-doctoral studies, he worked with Prof. Tim K. Minton, Montana State University, USA for a period of 2 years, in the area of reaction dynamics using cross beam technique during 2004-2006. His current research interests focus on photodissociation and reaction dynamics involving small polyatomic molecules as well kinetics of atmospherically important reactions in gas phase..*

Prakash D. Naik *was born in 1959 in Karwar, India. He received his B.Sc. in Chemistry in 1980 from Karnataka University, Dharwar, India and M.Sc. in Chemistry in 1983 from University of Mumbai, India. He is currently working as a Scientific Officer in Radiation & Photochemistry Division of Bhabha Atomic Research Centre, Mumbai, India. He received his Ph.D. degree in Chemistry from University of Mumbai in 1992. He worked for a period of 1.5 years at Institute of Physical Chemistry, University of Heidelberg, Germany in the area of photodissociation and reaction dynamics with Prof. J. Wolfrum during 1992–1993. His current research interests focus on laser-induced dissociation dynamics involving small polyatomic molecules and kinetics of atmospherically important reactions in gas phase.*

Obituary

Prof. Balu Venkataraman

(17 December, 1929 – 28 October, 2010)

Prof. Balu Venkataraman joined Bhabha Atomic Research Centre, then known as the Atomic Energy Establishment at Trombay after obtaining M.Sc. from Banaras Hindu University and a Ph. D. from Columbia University. However, he was fully associated with Tata Institute of Fundamental Research and spent nearly three decades there. He built a pulsed super-heterodyne and later a homodyne time-domain EPR spectrometer suitable for studying spin-lattice relaxations as well as spin dynamics of transient radicals produced by a pulsed laser. He was instrumental in establishing a pico-second time-resolved fluorescence laboratory at TIFR. Prof. Venkataraman realized the power of pulsed lasers in studying fast processes and in 1987, arranged a five-week long workshop on "Study of Fast Chemical Processes" at Lonavala. He made a series of television programmes on science and nature for Doordarshan's Tamil channel. Prof. Venkataraman was associated with ISRAPS since its inception and took the responsibility of posters evaluation in the Trombay Symposium of Radiation and Photochemistry and summarizing the Symposium at its concluding session. ISRAPS recognized his life-long work by bestowing a lifetime achievement award. Prof. Venkataraman passed away on 28th October 2010 after a brief illness. We, the members of ISRAPS deeply mourn his demise and may his soul rest in peace.

❖❖❖

Dr. B. L. Gupta

*(*9 November, 1939 – 21 January, 2010*)*

Dr. B. L. Gupta joined 7th Batch of AEET School after obtaining M. Sc. degree from University of Roorkee. After graduating successfully, he joined Radiochemistry Division in 1964 and later on shifted to Division of Radiation Protection. He obtained his Ph.D. degree from University of Bombay in 1972. He led a group of scientists on Chemical Dosimerty and developed several dosimetry techniques like glutamine dosimeter, plastic colour dosimeters etc. His work on extremely low level FBX chemical dosimeter is internationally recognized. He was associated with several international collaborations for dose inter-comparison methods and participated in several international symposia and meetings. He was chief investigator of three IAEA research contracts. He served various scientific bodies like AMPI, AERB in various capacities. He was executive council member and treasurer of ISRAPS during 1992-1999 and was actively involved in organizing National Symposium on Radiation & Photochemistry at Jabalpur and Vishakhapattanam. After retiring from BARC in 1999 he passed away after a brief illness on 21 January, 2010. We, the members of ISRAPS deeply mourn his demise and may his soul rest in peace.

❖❖❖

150th Birth Anniversary of Acharya P C Ray : Father of Indian chemistry

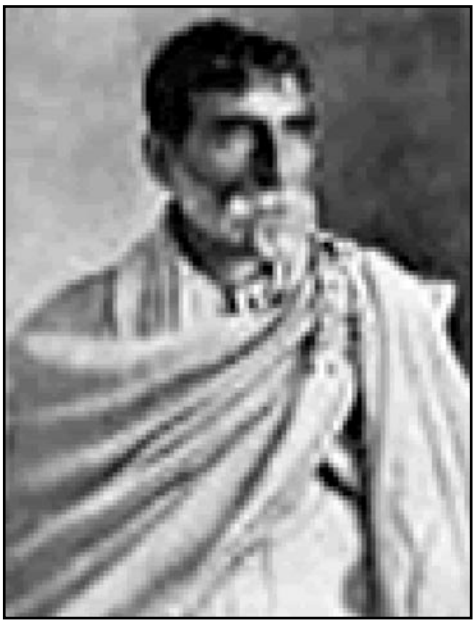

The late nineteenth and early twentieth century Bengal had witnessed the advent of a new intellectual and cultural reawakening, which is widely known as the Bengal Renaissance which had played a significant role in the independence of India and its progress towards a modern civilization. Among the many thinkers and intellectuals who made their notable contributions in this new literary, scientific and cultural renaissance, Acharya Prafulla Chandra Ray (1861-1944) and Rabindranath Tagore (1861-1941) are the most important to be mentioned, who sought to give India a new distinct and cognitive identity

Acharya Prafulla Chandra Ray was born on August 2, 1861 in Raruli. After attending Hare School and the Metropolitan College (now Vidyasagar College) where the lectures of Alexander Pedler attracted him to chemistry. After taking F.A. diploma (1881) from the University of Calcutta, he proceeded to the University of Edinburgh on a Gilchrist scholarship. Ray joined in 1889 a specially created post in the Presidency College where he served from 1889 to 1916.

Famous Indian scientists like Meghnad Saha, Bhatnagar, N.R. Dhar, J.C. Ghose were among his students. Ray had special interest in mercury because of its importance in Ayurvedic medicines. He discovered Mercurous Nitrite, when scientists did not know that such a chemical could exist. This result was published in 1896 in the Journal of Asiatic Society of Bengal. For this discovery he received congratulatory letters from many eminent chemists such as Bertheldt, Roscol and Victor Meyer. Another notable contribution made by Ray was the synthesis of ammonium nitrite in pure form.

Ray wrote more than 100 papers, some in collaboration with his students, on mercury salts and related compounds. He founded the Bengal Chemical and Pharmaceutical Works (1892), Bengal Pottery Works, Calcutta Soap Works and other factories, in the face of obstruction of the British to create jobs for the unemployed youths. On retiring from the Presidency College, he became the first Palit Professor of Chemistry in the University College of Science founded by Sir. Ashutosh Mukherjee. Here he continued his research and teaching for another two decades till 1937. In the Presidency College it was J.C. Bose and Ray, in the College of Science it became Raman and Ray. The trio Bose-Ray-Raman heralds the birth of modern science in India. He was the founder of the Indian chemical school.

Ray received many honours: honorary doctorates, C.I.E. (1911), Knighthood (1919), President of the Indian Chemical Society (1924). At the 70th birthday celebrations of Ray, poet Tagore praised his exemplary life: "in the Upanishads, we learn 'the One became Many". Acharya Prafulla Chandra has devoted his life to his students; he now lives in the hearts of many.

Ray passed away on June 16, 1944 at the age of 83 in his room in the college which he had occupied for twenty-five years. He was a great patriot and social worker.

Sisir K Sarkar

Structure & Dynamics of Complex Chemical Systems:
An Interface between Theory & Experiment

A Publication of Indian Society for Radiation & Photochemical Sciences

CONTENTS